



# Boreal Forest and Forest Fires

# 21

Yongwon Kim, Hideki Kobayashi, Shin Nagai, Masahito Ueyama,  
Bang-Yong Lee, and Rikie Suzuki

## Abstract

Boreal forest has played a role as sink of atmospheric CO<sub>2</sub> due to the slow growth of black spruce; however, changes in source of atmospheric CO<sub>2</sub> by forest fires and recent warming have significantly triggered modulation in physiological ecology and biogeochemistry over the boreal forest of Alaska. This chapter describes recent research findings in boreal forest ecosystem of Alaska: (1) the forest aboveground biomass (AGB) with field survey data and satellite data, (2) latitudinal gradients of phenology with time-lapsed camera and

---

Y. Kim (✉)

International Arctic Research Center, University of Alaska Fairbanks, Alaska, AK, USA  
e-mail: [kimywj@gmail.com](mailto:kimywj@gmail.com)

H. Kobayashi · S. Nagai · R. Suzuki

Japan Agency for Marine-Earth Science and Technology, Research Institute for Global Change, Institute of Arctic Climate and Environment Change Research, Yokohama, Japan  
e-mail: [hkoba@jamstec.go.jp](mailto:hkoba@jamstec.go.jp)

S. Nagai

e-mail: [nagais@jamstec.go.jp](mailto:nagais@jamstec.go.jp)

S. Nagai

Japan Agency for Marine-Earth Science and Technology, Research Institute for Global Change, Yokohama, Kanagawa, Japan

M. Ueyama

Graduate School of Life and Environmental Sciences, Osaka Prefecture University, Osaka, Japan

e-mail: [ueyama@envi.osakafu-u.ac.jp](mailto:ueyama@envi.osakafu-u.ac.jp)

B.-Y. Lee

Division of Polar Climate Sciences, Korea Polar Research Institute (KOPRI), Incheon, South Korea

e-mail: [bylee@kopri.re.kr](mailto:bylee@kopri.re.kr)

© Springer Nature Switzerland AG 2021

D. Yang and D. L. Kane (eds.), *Arctic Hydrology, Permafrost and Ecosystems*,  
[https://doi.org/10.1007/978-3-030-50930-9\\_21](https://doi.org/10.1007/978-3-030-50930-9_21)

615

satellite data, (3) spatio-temporal variation of leaf area index (LAI) with the analysis of satellite data, (4) latitudinal distribution of winter and spring season soil CO<sub>2</sub> emission, and (5) successional changes in CO<sub>2</sub> and energy balance after forest fires. As a result, mapping of forest AGB is useful for the evaluation of vegetation models and carbon stock in the biogeochemical cycle. Latitudinal distribution of phenology understands the recent and future phenological changes including post-fire recovery forests. Interannual variation of LAI shows the leaf dynamics and near-surface remote-sensing approaches with the analyses of time-lapsed digital camera and satellite data. Spring carbon contributions are sensitive to subtle changes in the onset of spring. Vegetation recovery after forest fire is the major driver of the carbon balance in the stage of early succession. Increasing soil carbon emission in response to abrupt climate warming in Alaska is a significant driver of carbon balance.

---

## 21.1 Introduction

Boreal forest, also called taiga that represents “a marshy forest in Siberia” in Russia, is the largest terrestrial ecosystem on Earth, covering 17% of the planet’s land surface area in a circumpolar belt of far Northern Hemisphere (Apps and Prices 1996; Kasischke and Stocks 2000). Boreal forest contains approximately 66% of the world’s forest soil carbon pools (Van Cleve et al. 1983; Billings 1997; Oechel and Vourlitis 1997; Kasischke and Stocks 2000). Because boreal forests absorb atmospheric carbon dioxide and slowly decompose the litter, fibric, and humic substances, the ecosystems are known as carbon sinks (Schlesinger 1997; Fan et al. 1998). Boreal forest is found throughout the high northern latitudes, between the tundra and the temperate forest, from about 50°N to 70°N, stretching across the interiors of Siberia, northern Asia, and northern Europe, and occupying millions of acres of North America. Also, boreal forest is characterized by the dominantly coniferous species like pine (*Pinus*), spruce (*Pices*), larch (*Larix*), and fir (*Abies*), and deciduous species such as birch (*Betula*), poplar/aspens (*Populus*), and alder (*Alnus*). Understory plants of boreal forest are inhabited different kinds of shrubs, mosses, lichens, and ferns (Vitt et al. 1988; Johnson et al. 1995). These species have adapted to short growing seasons with long days and very cold winters with short days and persistent snowpack. Further, discontinuous permafrost, dominating 50–90% of boreal forest, distributes under the boreal coniferous forests that are situated in the north slope of forests (AMAP 2017).

In Alaska, boreal forest exists in the Interior Alaska lands between the Brooks Ranges in the north and the Alaska Ranges in the south. At higher elevations within the broad range of the boreal forest ecosystem are pockets of alpine tundra vegetation, and along the margins of the ranges, it intergrades with lowland or arctic tundra. Black spruce communities are widely distributed in boreal Alaska. Around 30–40% of Alaska’s landscape is boreal black spruce forest (Barney and Stocks

1983), which is the most common boreal forest type in Interior Alaska (Viereck et al. 1992; Cronan et al. 2012). Alaskan black spruce communities typically occur on cold, poorly drained, nutrient-poor sites with a shallow permafrost layer; hence, the productivity is usually low (Viereck et al. 1992). The most common black spruce types are broadly divided into upland and lowland types. Typically, upland types occupy low gradient or north slopes, while lowland types occupy broad valleys or old river terraces. Less common types are productive black spruce forests on south slopes and black spruce-lichen woodlands.

Forest fire, which is largely controlled by local weather and vegetation, is a major disturbance in boreal forests with its occurrence closely coupled to climate patterns. Therefore, changes in climate will result in change in the fire regimes. Although boreal forests are presently one of the major terrestrial carbon pools, shifts in the fire regime and ecosystem distribution in high latitudes associated with climate change are likely to result in significant increases in atmospheric concentrations of carbon dioxide and other greenhouse gases (Kasischke et al. 1995, 2000a, b; Kasischke 2000; Richter et al. 2000; Kim and Tanaka 2003; Himzman et al. 2003). As boreal forests emit higher concentrations of carbon to the atmosphere immediately after the fire, forest fires in the northern stands are well known as carbon sources (Seiler and Crutzen 1980; Crutzen and Andreae 1990; Levine 1991; Kasischke et al. 2000b, c). Hansen et al. (1996) showed that, based on the average temperature over the past 30 years, the most significant areas of warming coincide with the region occupied by the boreal forest. Given the close linkage between fire occurrence and climate, there should be little surprise that over the past two decades, there has been a significant increase (almost threefold) in the annual area burned in the North American boreal forest (Kasischke and Stocks 2000). Interestingly, boreal black spruce communities need the fire by alternatively lightning and/or human-cause for the next generation. The survival strategy of black spruce forest is to (1) dangle the cones in the top of stem, (2) ignite the dead branches as a fuel in the bottom stem by the fire, (3) move a fire from bottom to top of stem, (4) activate the cones by a fire, (5) open physiologically the cones after the extinguishment, and (6) scatter the seeds by wind and settle down the seeds on the burned soil surface for seeding. The forest fire is called “crown fire” in boreal black spruce communities. On the other hand, the fire in larch forest of Siberia is “ground fire”. Fire return time ranges from 50 to 500 years (Yarie 1981; Dyrness et al. 1986; Kasische et al. 1995; Kasischke and Stocks 2000; Lynch et al. 2003). This fire regime is highly variable because of its sensitivity to vegetation, topography, climate (especially short-term extreme fire-weather events), and human activities (as both a source of ignition and an agent of fire control) (Kasischke et al. 1995; Stocks et al. 2003; Dissing and Verbyla 2003).

Alaska fire history since 1940 is concentrated in boreal forest, Interior Alaska between Alaska Ranges and Brooks Ranges (Fig. 21.1). It is clear that boreal forest of Alaska has ever damaged by the forest fire. Hence, recent boreal forests are mostly the secondary forest regenerated through the ecologically successional stages after the forest fires.

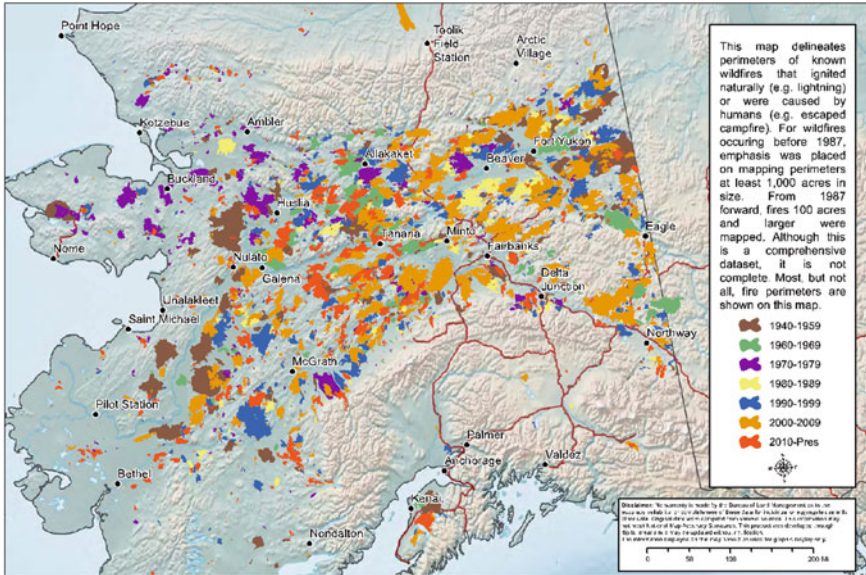


**Fig. 21.1** Alaska fire history from 1940 to present Alaska Interagency Coordination Center (2018)

In this chapter, we describe recent research and understanding of: (1) the change in aboveground biomass with the analysis of field data and remote-sensing satellite data, (2) the latitudinal gradients of snow-on and snow-off dates with time-lapsed camera and remote-sensing data, (3) the spatio-temporal variations of normalized deviation vegetation index (NDVI) and leaf area index (LAI), (4) spatial distribution of winter and spring soil CO<sub>2</sub> emissions along the trans-Alaska pipeline, and finally (5) changes in carbon with soil chamber and eddy covariance tower methods in Interior Alaska after forest fire.

## 21.2 Recent Research and Results

### 21.2.1 Changes in Aboveground Biomass (AGB)

The carbon assimilation in woody components in boreal forests contributes to mitigate the global carbon cycles (IPCC 2014). Assimilated carbon in woody (forest biomass) represents the available biological resources. Wildfires alter boreal forest landscapes in Interior Alaska, thus causes the long-term changes in forest biomass distribution. Remote-sensing technologies are expected to provide the geographical patterns in forest biomass distribution from space. In remote-sensing observation, forest biomass specifically indicates the dry weight of biomass. As the remote-sensing techniques are only able to apply for the targets seen from satellite,

aboveground biomass (AGB) is often used as the representative term. AGB is further divided into trunk, branch, and leaf biomasses and their allometries depend on the tree species.

Microwave synthetic aperture radar (SAR) is one of the promising remote-sensing information for AGB estimation. SAR is an active microwave sensor. The emitted microwave pulses from the orbital satellite antennas reach to the Earth's surface and is backscattered. The intensity of the backscattered signal contains the land surface structure such as forest characteristics including AGB (e.g., Ulaby et al. 1986; Belchansky 2004). Because microwaves are less affected by cloud cover, SAR technology provides the all-weather signals in regions where cloud cover is high, such as boreal forest regions. The SAR backscatter is characterized by the polarized (horizontal or vertical) combinations of the transmitted and received signals. The "HH" mode indicates the combination of a horizontally (H) polarized transmitted signal and a horizontally (H) polarized received signal. "HV" stands for the combination of a horizontally polarized (H) transmitted signal and a vertically polarized (V) received signal. Generally, the sensitivity of the backscatter intensity to the biophysical parameters of land surface vegetation is examined in different combinations of polarized modes. The L-band SAR data have been used for the AGB estimation from tropical to boreal forest ecosystems (Suzuki et al. 2013). The forest regrowth monitoring after the fire disturbance was also explored (Kasischke et al. 2011). However, current SAR-based AGB estimation methods rely on the regression between SAR signals and ground-based AGB samples. Therefore, the ground-based AGB surveys with diverse forest growth stage are of particular importance.

Tree census survey is the most common approach to obtain canopy height, diameter of breast height (DBH), and other ancillary information and thus is the best method to obtain reliable AGB at site scale. However, tree census survey is very labor-intensive, which impede to conduct the data acquisition from multiple sites, such as post-fire regrowth to mature stage forests. The Bitterlich angle-count sampling method is a sampling method of the total basal area within the forest plot. By combining the Bitterlich method with allometry equation, AGB is also estimated. Details of this method are summarized in Osumi (1987) and Nagumo and Minowa (1990). The Bitterlich survey only takes approximately 30 min for one forest plot, thus it enables to obtain the AGB from various forest stands. Figure 21.2 shows the geographical distribution of Bitterlich sampling locations in Interior Alaska, along the Dalton Highway from Fairbanks (64° 51'N, 147° 51'W) to the foothill of Brooks Ranges (67° 59'N, 149° 45'W).

The AGBs listed in Table 21.1 are the summary of the Bitterlich survey for the 29 locations. Allometric equations derived by Yarie et al. (2007) were used for the AGB calculation of the dominant tree species in Interior Alaska. In addition to the Bitterlich surveys, conventional census survey (the fixed plot method) is performed at the site #8. Thus, DBH and tree height measurements of all trees (284 tree stands) in the 25 m by 25 m plot were performed. From the comparison of two approaches, it is found that the AGB estimation by the Bitterlich method was slightly higher than that of the fixed plot method (4–22%). However, the difference was fairly

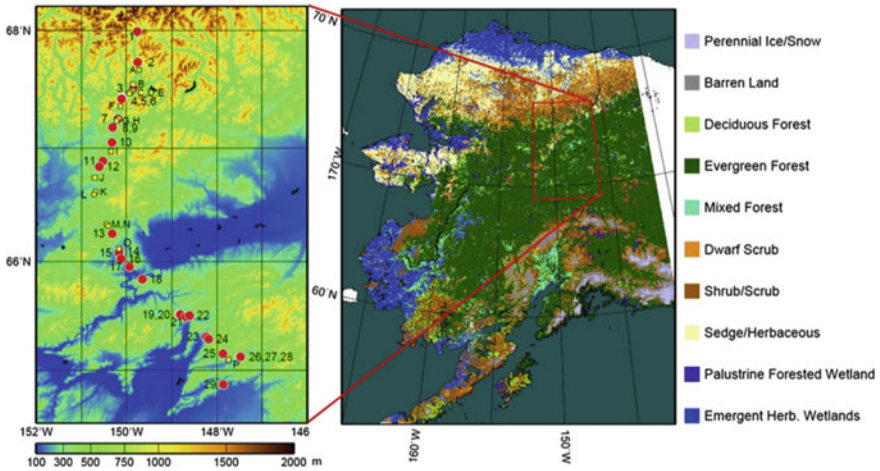


**Fig. 21.2** The 29 sampling forest locations (red circles) and the 16 non-forest sites for the background information (yellow dots) in Interior Alaska (left). The land cover is classified according to the U.S. National Land Cover Database 2001 (right) (after Suzuki et al. 2013)

small, suggesting the multi-site Bitterlich surveys are reliable around the site #8. Due to severe climate situations, AGBs from the spruce forest sites were generally small. The range of AGBs and tree densities were from  $2.2 \text{ Mg ha}^{-1}$ , to  $1266 \text{ trees ha}^{-1}$  (site #5) and  $116.2 \text{ Mg ha}^{-1}$  to  $814 \text{ trees ha}^{-1}$  (#16). The fire history affects the spruce forest structures. The forest site #17 was a relatively young forest after wildfires and was the densest ( $11263 \text{ trees ha}^{-1}$ ), medium AGB ( $81.7 \text{ Mg ha}^{-1}$ ), and low tree height (average = 5.9 m).

The phased array type L-band synthetic aperture radar (PALSAR) onboard the advanced land observing satellite (ALOS) is one of L-band microwave SAR sensor. The sampling footprint is 20 m by 10 m (Rosenqvist et al. 2007). The digital number (DN) values (arbitrary backscattering intensity) from two polarization modes (HV and HH) were converted to a normalized radar cross-section (NRCS), that is,  $\sigma_{\text{HV}}^0$  and  $\sigma_{\text{HH}}^0$ . Details for the NRCS calculation were provided in Suzuki et al. (2013) and Shimada et al. (2009). The 20 scenes were merged into one continuous image, then manually identified the forest locations of the 29 forest and 16 non-forest (background) sites on the PALSAR images by visual interpretation. The relationship between  $\sigma_{\text{HV}}^0$  and AGB was regressed by logarithmic function. Figure 21.3 shows regression curvature for two polarization data sets (HV and HH). When regressing, the saturation level of the forest AGB has to be determined. The saturation level was defined as the value of AGB when the slope of the logarithmic regression curve decreased to 0.02 dB against 1% of the range (minimum to maximum) of the AGB obtained by the field survey.

The scatter-diagrams and logarithmic regression equations in Fig. 21.2 demonstrate the fitness of the relationships between the in situ forest AGB and satellite

**Table 21.1** Location (latitude and longitude) of the forest sites, dominant tree species, and forest aboveground biomass (AGB)

Site ID	Latitude (N)	Longitude (W)	Dominant tree species	Forest AGB (Mg ha <sup>-1</sup> )	Tree density (ha <sup>-1</sup> )
1	67° 59'	149° 45'	White spruce	4.8	795
2	67° 44'	149° 45'	White spruce	31.9	740
3	67° 30'	149° 50'	White spruce	27.5	1228
4	67° 26'	150° 05'	White spruce	25.4	2063
5	67° 25'	150° 06'	White spruce	2.2	266
6	67° 25'	150° 06'	White spruce	20.8	1519
7	67° 15'	150° 11'	Black & white spruce	5.8	974
8	67° 10'	150° 17'	Black spruce	22.4	4740
9	67° 10'	150° 18'	Black spruce	35.0	2960
10	67° 02'	150° 19'	Black & white spruce	12.3	1475
11	66° 53'	150° 31'	Black spruce	4.3	1261
12	66° 50'	150° 36'	White spruce	69.8	916
13	66° 14'	150° 18'	Black & white spruce	24.8	2561
14	66° 05'	150° 09'	Black spruce	7.3	3035
15	66° 04'	150° 09'	Black spruce	12.6	2895
16	66° 01'	150° 07'	White spruce	116.2	814
17	65° 57'	149° 56'	Black spruce	81.7	11263
18	65° 50'	149° 38'	Black spruce	30.8	3848
19	65° 31'	148° 49'	Black spruce	66.9	7430
20	65° 31'	148° 48'	Black spruce	36.0	4269
21	65° 29'	148° 41'	Black spruce	40.1	5342
22	65° 30'	148° 36'	Black spruce	16.3	1403
23	65° 18'	148° 14'	Birch	100.2	946
24	65° 17'	148° 10'	Birch & white spruce	92.7	3292
25	65° 09'	147° 52'	Black spruce	15.3	1546
26	65° 07'	147° 29'	Black spruce	50.7	6013
27	65° 07'	147° 28'	Black spruce	6.6	1665
28	65° 07'	147° 28'	Black spruce	12.7	873
29	64° 51'	147° 51'	Black spruce	12.8	3432

signals ( $\sigma_{HV}^0$  and  $\sigma_{HH}^0$ ). Because the in situ forest AGB values are weighted in a small size AGB range within 0 to 40 Mg ha<sup>-1</sup>, the regression curvatures are highly skewed due to this clumped data. In order to overcome this issue, the regressions were performed with average AGB for each 5 Mg ha<sup>-1</sup> AGB class denoted as open

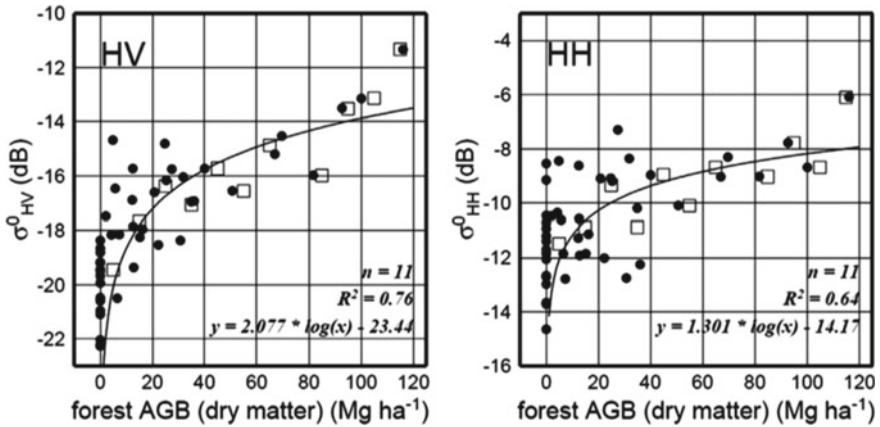


**Fig. 21.3** Relationship between the in situ forest AGB and  $\sigma_{\text{HV}}^0$  (left) and  $\sigma_{\text{HH}}^0$  (right) of ALOS/PALSAR. Closed circles are the original values of the 45 sites. Open squares denote the mean  $\sigma^0$  value for each forest AGB class ( $5 \text{ Mg ha}^{-1}$  interval) (after Suzuki et al. 2013)

squares in Fig. 21.2. This demonstrates that the saturation level of  $\sigma_{\text{HV}}^0$  is higher than that of  $\sigma^0$ .

The spatial distribution of forest AGB was estimated from ALOS/PALSAR data and the regression equations (Fig. 21.3). The geographical and latitudinal distribution of the forest AGB (Fig. 21.4) are presented well in the AGB map, but some erroneous values due to “foreshortening” cannot be avoided in the slope surfaces (e.g., Shimada 2010). Although the accurate correction of the slope effect is challenging, the slope correction improves the spatial representativeness of the AGB in Interior Alaska. Maps of forest AGB can be useful for the evaluation of forest ecosystem and vegetation models (Le Toan et al. 2004). AGB maps are also useful to evaluate the carbon stock in the context of the global biogeochemical cycle in pre- and post-fire landscapes.

### 21.2.2 Multi-scale Phenology Observation in Boreal Forest Ecosystems

Phenology is defined as recursive events of plants. Leaf, flower, and other activities have their own phenological patterns. Seasonal leaf area changes are useful information in the context of terrestrial carbon cycles and climate change. Reliable evaluation of start of growing season (SOS), end of growing season (EOS), and growing season length is essential to understand how terrestrial vegetation responds to climate changes (Buermann et al. 2014; Keenan et al. 2014; Nagai et al. 2013; Piao et al. 2011; Richardson et al. 2013a; Schwartz et al. 2013; Verbyla 2008; Xu et al. 2013). It is also important to understand how forest fires alter the plant species

compositions, their recovery, and phenology timings (Tsuyuzaki et al. 2009, 2013; Kobayashi et al. 2016). In boreal forests and tundra regions, there are several evidences that the SOS timings were advanced (Buermann et al. 2014; Delbart et al. 2008; Hogda et al. 2013; Myneni et al. 1997; Piao et al. 2011). On the other hand, trends in EOS are less studied due to very limited ground-based information (Jeong and Medvigy 2014). Some recent studies showed a trend for later EOS in Europe (Garonna et al. 2014), North America (Zhu et al. 2012), and for temperate vegetation over the northern hemisphere (Jeong et al. 2011). However, it is not clear whether the environmental factors (e.g., photoperiods and temperature changes) actually influence the changes in EOS (Delpierre et al. 2009; Jeong and Medvigy 2014; Richardson et al. 2013b).

Satellite observation is necessary to quantify the actual plant phenology over large area. The satellite estimation utilizes the vegetation indices such as normalized difference vegetation index ( $NDVI = (NIR - Red)/(NIR + Red)$ ), where NIR and Red are reflectances in near-infrared and red spectral regions. Satellite method provides the continental scale geographical patterns in phenology. However, several issues remained. First, SOS and EOS estimated to quantify how much spring snowmelt and autumn snow condition affects the satellite signal and phenology retrievals. Second, frequent cloud appearance prevents from retrieving the sufficient number of surface reflectances, making it difficult to determine phenology timings.

Boreal forests in Alaska are extremely sparse. Large amount of sunlight reaches the understory layer, making the understory layer bright. In other words, understory plants greatly affect the phenology and seasonality obtained by satellite (Pisek and Chen 2009; Rautiainen and Heiskanen 2013; Yang et al. 2014). In Interior Alaska, evergreen needles such as black and white spruce are the dominant species. Satellite phenology observation is greatly influenced by understory plant phenology. However, the effect of overstory and understory on satellite-based phenology is less investigated. Recent time-lapse camera networks enable to obtain the ground-truth of the phenology timings in various forest and tundra conditions including post-fire locations.

Alaskan boreal forest and tundra are located from a latitudinal range of 61°N–71°N (Fig. 21.5). This region is divided into two distinct ecosystems. Lower latitude zone (61°N–68°N) is covered by the evergreen coniferous and deciduous forests. The dominant tree species in the boreal zone is black spruce (*Picea mariana*). White spruce (*Picea glauca*) and aspen (*Populus tremuloides*) are also common (Chapin III et al. 2006). The understory layer is covered with rusty peat moss (*Sphagnum* spp.) and splendid feather moss (*Hylocomium splendens*). These species show highly variable colors (brown to green) spatially and seasonally. The understory layer is also partly covered with “tussocks”. It consists of herbaceous perennial cotton grass (*Eriophorum vaginatum*) (Kim et al. 2013). The low shrubs and herbs such as Labrador tea (*Ledum groenlandicum*), bog bilberry (*Vaccinium uliginosum*), dwarf birch (*Betula nana*), and cloudberry (*Rubus chamaemorus*) are dominant deciduous vascular plants. Tundra is further divided into heath tundra and moist acidic tundra areas. The moist acidic tussock tundra is dominated by tussock

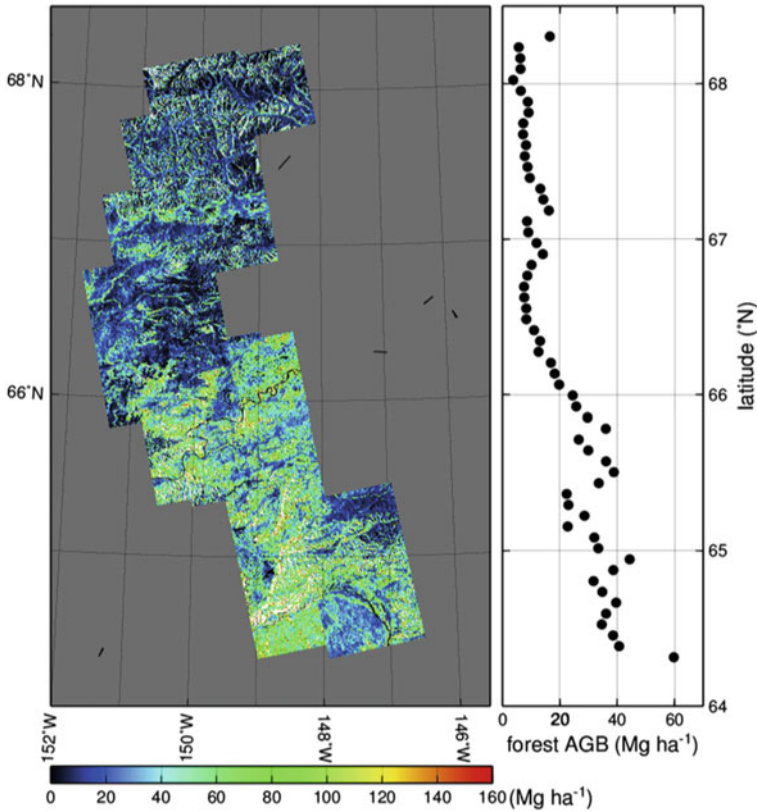
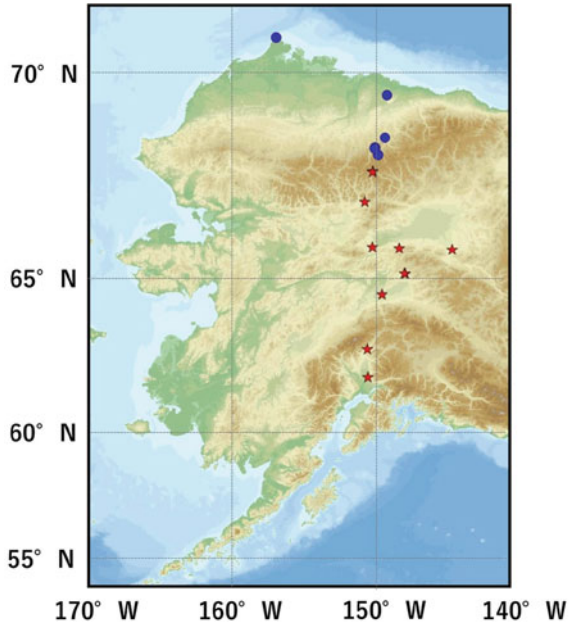


**Fig. 21.4** Forest AGB distribution in Interior Alaska as estimated by ALOS/PALSAR backscatter intensity (HV) in summer of 2007 (Left). The latitudinal gradient of forest AGB (right) (after Suzuki et al. 2013)

sedge (*Eriophorum vaginatum*) and dwarf shrubs (*Betula nana*, *Carex bigelowii*, *Vaccinium vitis-idaea*, and *Ledum palustre*) (Euskirchen et al. 2012; Kim et al. 2014; Oechel et al. 2014). The dry heath tundra is dominated by *Dryas* spp., lichen, and dwarf shrubs (Euskirchen et al. 2012).

Time-lapse camera is a useful tool to track the seasonality of surface conditions. It has been widely used for the determination of phenological timings (Richardson et al. 2007; Woebbecke et al. 1995). The time-lapse camera system was used to quantify the phenology at 17 sites across Alaska (Fig. 21.5). The six northern sites are located in tundra and the other 11 sites are in boreal forests. In boreal forest sites, there is a site that was experienced by the large forest fire events in 2004 (Iwata et al. 2011, 2013). At these sites, there are three different time-lapse camera systems: GardenWatchCams (Brinno Inc., Taiwan), webcams, and a fish-eye camera (Nikon Coolpix 4500 with an FC-E8 fisheye lens). These camera systems

**Fig. 21.5** Ground-based time-lapse camera locations in Interior Alaska and tundra zones



viewed the tundra and forest understory vegetation at a nadir or horizontal view with a sampling interval from 15 min to 6 h.

There are several global environmental satellites such as NOAA's Advanced Very High Resolution Radiometer (AVHRR), Moderate resolution imaging spectroradiometer (MODIS) on Terra and Aqua, SPOT-VEGETATION, Prova-V, and more recently Suomi-NPP's Visible Infrared Imaging Radiometer Suite (VIIRS), European Sentinel series (Sentinel-2 & 3), and Japanese Global Climate Observation Mission (GCOM-C). These satellites measure and produce a global terrestrial coverage every two- to three-day interval. To screen out the cloud-contaminated measurements in the surface reflectance data, 8–10 days compositing is common, which is the method to extract the best quality of a sampling within a compositing period. The NDVI and normalized difference infrared index (NDII) were widely used for the phenology estimations, where  $NDII = (NIR - SWIR)/(NIR + SWIR)$  and SWIR is a shortwave infrared (wavelength of  $\sim 1.6 \mu m$ ). There are several satellite algorithms to determine SOS and EOS, for example, local NDVI threshold method (White et al. 1997), the NDII method (Delbart et al. 2005), and the sigmoid method (Zhang et al. 2003).

The phenology and snow cover conditions can be estimated by both satellites and time-lapse images. Figure 21.6 is the estimated phenology (SOS and EOS) and snow timings (snowmelt and continuous snow cover dates) in 2011. Phenology in boreal evergreen forest indicates the spring leaf emergence and autumn senescence timing of understory plants. The snowmelt in spring comes 16–19 days earlier than SOS estimated by the time-lapse camera and the satellite method. In autumn, the

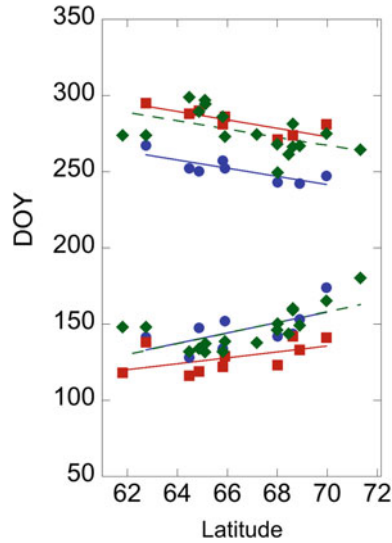


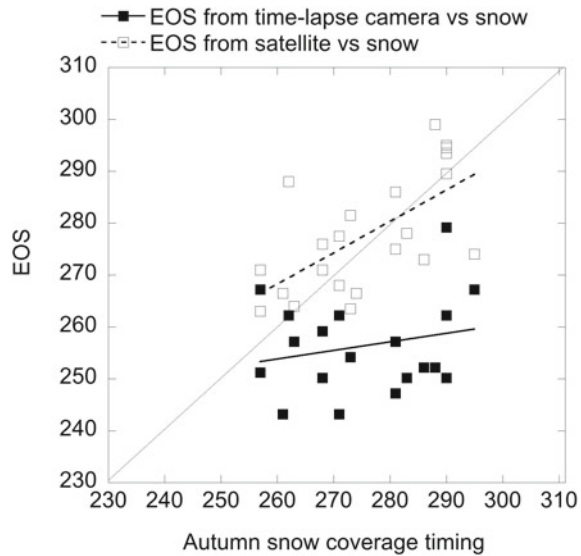
**Fig. 21.6** Latitudinal gradients of SOS and EOS derived from satellite (green closed diamond) and time-lapse camera (blue open circle). The snowmelt and autumn snow coverage are also depicted (red closed square). The satellite SOS and EOS are derived by the average of three methods (the local threshold method, the NDII minimum method, and the sigmoid fitting method) from two satellites (Terra-MODIS and SPOT-VEGETATION). Details are provided in Kobayashi et al. (2016)

satellite EOS comes almost in the same timing with autumn snow coverage. However, the satellite EOS was 19–26 days later than the EOS by time-lapse camera. This result suggests that satellite EOS is mostly affected by the autumn snow events rather than the plant phenology (Fig. 21.6).

In spring phenology, satellite-based SOS is known to be partially affected by the snowmelt in boreal forests and tundra zones. Despite this issue, the satellite-based SOS may be related to leaf emergence in spring because leaf emergence (SOS) occurs soon after the snowmelt. The SOS accuracy depends on the degree of synchronism in snowmelt and leaf emergence timings.

For the EOS timings, camera-based EOS is not correlated well with the satellite-based EOS. The satellite-based EOS was more related to the timings of autumn snow coverage whereas the camera-based EOS was not entirely correlated with autumn snow coverage (Fig. 21.7). These results show the potential utility and limitation of the satellite-based phenology observation and also a usefulness of time-lapse camera networks. The rising temperature in the northern high latitudes is abrupt and strong. Regarding the key issues of boreal ecosystems in the context of climate change, plant phenology, spring green-up, and autumn senescence are essential information for regional and global carbon cycle. The satellite and

**Fig. 21.7** The relationship between the autumn snow coverage timing and EOS. The correlation coefficients for the EOS from satellite and EOS from time-lapse camera are  $R = 0.63$  ( $p = 0.017$ ) and  $R = 0.19$  ( $p = 0.88$ ), respectively



ground-observation networks are thus very important in order to understand the future phenological changes including post-fire recovery forests.

### 21.2.3 Interannual Variations of Northern LAI

Leaf area index (LAI) is defined as one half of the total leaf area per unit of horizontal ground area ( $\text{m}^2 \text{m}^{-2}$ ). The annual maximum LAI in open-canopy forests in Alaska (with low aboveground biomass) is smaller than that in closed-canopy tropical forests (with high AGB) (Myneni et al. 2002; Zhu et al. 2013; Iio et al. 2014). In association with the characteristics of the timings and patterns of plant phenology, such as leaf-flush and leaf-fall among ecosystems and tree species, LAI shows interannual and seasonal variations (Nasahara et al. 2008; Muraoka et al. 2013; Nagai et al. 2017). Plant phenology affects carbon, water, and energy cycles through the  $\text{CO}_2$  uptake by photosynthesis, latent and sensible heat by evapotranspiration, surface albedo, and aerodynamic roughness of land surface (Richardson et al. 2013a). To better understand the interaction between ecosystems and climate change in Alaska, accurate detection of spatio-temporal LAI variability is an important but challenging task.

LAI in forest ecosystems can be estimated by the direct method (e.g., counting leaves and leaf litter collection approaches; Eschenbach and Kappen 1996; Nasahara et al. 2008; Potitthep et al. 2013; Iio et al. 2014; Nagai et al. 2017) and indirect method (i.e., near-surface and satellite remote-sensing approaches; Eschenbach and Kappen 1996; Myneni et al. 1997, 2002; Ueyama et al. 2006, Kobayashi and

Iwabuchi 2008; Nasahara et al. 2008; Ryu et al. 2010; Richardson et al. 2011; Muraoka et al. 2013; Potitthep et al. 2013; Zhu et al. 2013).

Direct method is the “counting leaf” approach, that is, to count the number of leaves within a target area from the canopy-access tower and measure the mean area of sampling leaves by using a leaf area meter. The LAI is then estimated by mean leaf area and number of leaves for a target area (Eschenbach and Kappen 1996). In the “leaf litter collection” approach, we divide the dry weighted leaf litter, which was sorted into each tree species, by the leaf mass per area (LMA) of each tree species. Seasonal variation in LAI for each tree species can be estimated by collecting and sorting leaf litter four or five times in autumn (Nasahara et al. 2008; Potitthep et al. 2013; Nagai et al. 2017). On the other hand, we can evaluate LAI in spring by examining the relationship between LAI in autumn and seasonality of leaf phenology data, such as number of leaves per shoot and a leaf size for each tree species, which were periodically observed during a leafy period (Nasahara et al. 2008; Potitthep et al. 2013; Nagai et al. 2017). The total LAI of overstory and understory tree species can be estimated by adding LAI for each tree species. Direct method allows obtaining nearly true value, but we require the canopy-access tower for counting the number of leaves and measuring leaf size, and field surveys are also not labor-intensive. For these reasons, it’s not so easy to apply direct methods to multiple points.

The non-destructive “near-surface and satellite-remote sensing” approach is useful to evaluate LAI over a wide area. In the “near-surface remote-sensing” approach, LAI was estimated by measurement of the incident photosynthetically active photon flux density (PPFD) above the forest canopy and on the forest floor (Muraoka et al. 2013), analysis of digital hemispherical photography images (Ryu et al. 2010; Richardson et al. 2011), and measurement of the LAI-2000/2200C Plant Canopy Analyzer (Li-Cor Inc., USA; Ueyama et al. 2006; Nasahara et al. 2008; Ryu et al. 2010; Richardson et al. 2011). These methods are theoretically based on the “Monsi-Saeki theory” (Hirose 2005), which consists of the exponential relationship between the attenuation of light transmittance and stratification of plant biomass (leaves, stem, and branch). The estimated LAI in a leafy period is equal to plant area index (PAI), which includes leaves, stems, and branches. To estimate accurate LAI in forests, we should subtract the estimated LAI in a leaf-less period from the estimated LAI in a leafy period (i.e., PAI). However, non-destructive “near-surface remote sensing” approach allows estimating the interannual and seasonal variations in LAI at multiple points, where there are no canopy-access towers.

In an open-canopy black spruce (*Picea mariana*, evergreen coniferous) forest in Alaska, LAI above ground measured by the LAI-2000 Plant Canopy Analyzer was 2.4, while LAI above 1.0 m (i.e., measurement of only overstory vegetation) was 0.1–0.5 without a clear seasonality (Ueyama et al. 2006). The forest floor (i.e., understory vegetation) is covered by mosses and lichens (Ueyama et al. 2006). Accurate LAI in a forest ecosystem is the sum of understory (shrub and herb) and overstory vegetation (canopy trees). For this reason, the light transmittance above 1.0 m, which is a general measurement height of the LAI-2000/2200C Plant

Canopy Analyzer, causes underestimation of LAI in open-canopy forests. To estimate accurate LAI in open-canopy forests, at least we should measure the light transmittance above ground rather than above 1.0 m. We should also concern about the heterogeneity of understory and/or overstory vegetation at each measurement point.

In the “satellite remote-sensing” approach, LAI was estimated by the radiative-transfer model inputting the surface reflectance data (Kobayashi and Iwabuchi 2008) and by the empirical regression model based on the relationship between LAI and normalized difference vegetation index (NDVI) (Myneni et al. 1997; Potitthep et al. 2013). In the former, we examine the relationship among azimuth angle of satellite sensor, solar zenith and azimuth angles, characteristic of canopy structure, and surface reflectance data observed by satellite remote sensing. We then theoretically estimate the LAI through its relationship. In the latter, we estimate the LAI by applying the NDVI–LAI relationship to satellite-observed NDVI. To develop the accuracy of both methods, we require abundant ground-truth in multiple points in various forest ecosystems for input, calibration, and validation parameters.

We can use long-term global LAI data sets estimated by the satellite remote sensing such as “LAI3g” (<http://cliveg.bu.edu/modismisr/lai3g-fpar3g.html>, 15-day temporal frequency, 1/12 degree spatial resolution, temporal span of July 1981 to December 2011, Zhu et al. 2013) and “MOD/MYD15 Leaf Area Index” ([https://modis.gsfc.nasa.gov/data/dataproduct/dataproducts.php?MOD\\_NUMBER=15](https://modis.gsfc.nasa.gov/data/dataproduct/dataproducts.php?MOD_NUMBER=15), 8-day temporal frequency, 1 km spatial resolution, temporal span of February to current, Myneni et al. 2002). The “LAI3g” and “MOD/MYD15” data sets were used in canopy surface reflectance data observed by AVHRR sensors mounted on NOAA satellite series and MODIS sensors mounted on Terra and Aqua satellites, respectively. However, the canopy surface reflectance data in open-canopy forests in Alaska detect both understory and overstory vegetation, while that in closed-canopy forests in tropics detect only canopy-surface overstory vegetation. This fact indicates an importance that discrimination between LAI of understory vegetation (LAI<sub>u</sub>) and that of overstory vegetation is required to estimate accurate LAI in forest ecosystems on a global scale.

In an open-canopy evergreen coniferous forest in Alaska, seasonal variation in LAI is affected by plant phenology in understory vegetation, which showed clear interannual and seasonal variations (Fig. 21.8). Leaf-flush and leaf-fall in understory vegetation occurred late May (around day of year (DOY) 145) and middle September (around DOY 260), respectively. For instance, the timing of leaf-flush in understory vegetation in 2013 was later than other years, while the year-to-year variability of the timing of leaf-fall in understory vegetation was not so clear. In the high-altitude regions, satellite view angle and snow cover affected the seasonal variation in canopy surface reflectance data (Kobayashi et al. 2016). These facts suggest a possibility that canopy surface reflectance data including non-phenological elements mislead seasonal variation in LAI. To estimate the LAI<sub>u</sub>, the understory NDVI (NDVI<sub>u</sub>) was first retrieved in boreal forests using satellite-observed bidirectional reflectance distribution function data (Yang et al.

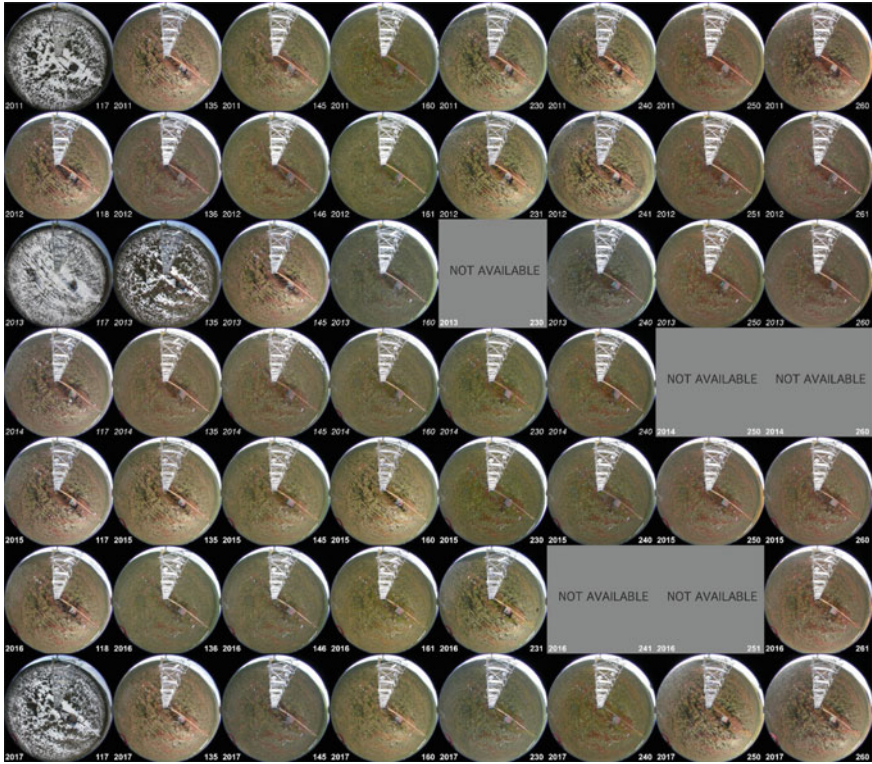


**Fig. 21.8** Year-to-year variability of typical canopy surface images from April 2009 to September 2017 in an open-canopy evergreen coniferous forest in Alaska: Poker Flat Research Range site ( $65^{\circ}7'24''\text{N}$ ,  $147^{\circ}29'15''\text{W}$ , 210 masl; Nagai et al. 2018, <http://pen.jamstec.go.jp/>). Year and day of year were shown in the left bottom and right bottom in each canopy surface image, respectively

2014), then the LAI<sub>u</sub> was estimated from NDVI<sub>u</sub> through a look-up table generated by the radiative-transfer model (Yang and Kobayashi 2018). Figure 21.9 shows an example of the estimated monthly average LAI<sub>u</sub> for boreal forests in July 2010.

To develop estimation of spatio-temporal variability of LAI in various ecosystems in Alaska, the following two tasks should be considered: (1) accurate detection of spatio-temporal variability in the timing of snowmelt, leaf-flush, leaf-fall, and snow on date, and (2) collection of ground-truth of LAI, plant phenology, and stratification of forest structure in multiple points. The timing of snowmelt is important for plant phenology in understory vegetation in Alaska although the consistency between the year-to-year variability in snowmelt dates and time of leaf-flush may not be assured. The timing of leaf-flush and leaf-fall also affects estimation of the interannual and seasonal variations in LAI.

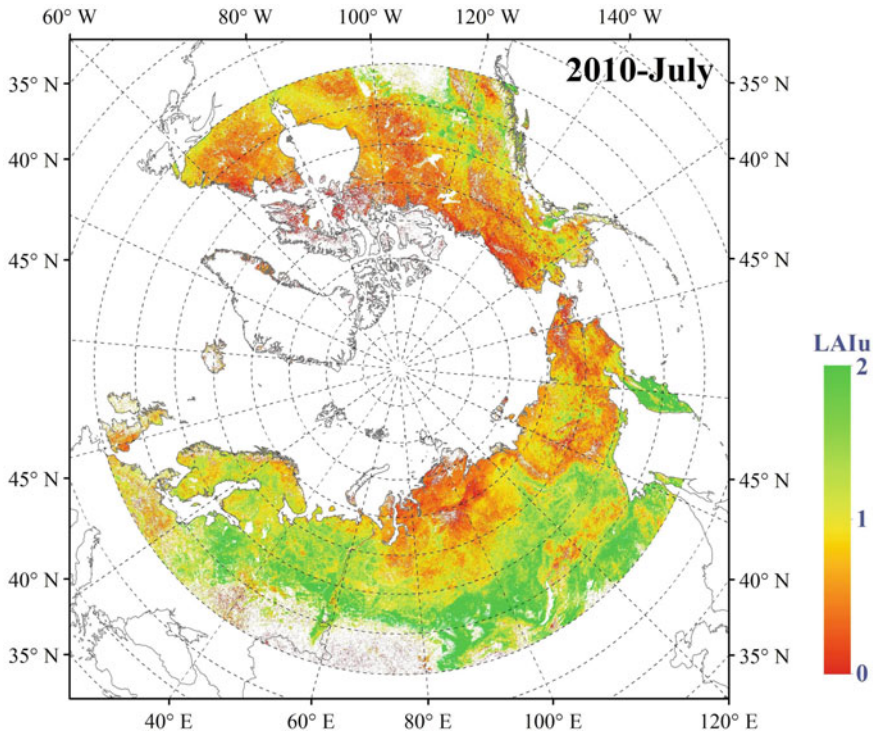


**Fig. 21.9** Spatial distribution of understory LAI (LAIu) in July 2010 in Pan-Arctic ecosystems (Yang et al. unpublished data)

To detect the spatio-temporal variability in leaf-flush and leaf-fall timing in Alaska, analysis of the time-series in daily satellite-observed vegetation index is useful. Although the definition of the timing of leaf-flush and leaf-fall by satellite-based analysis was not consistent with that by in situ observations, we can evaluate the spatio-temporal variability of the timing of start and end of growing season (Fig. 21.10), as the timing of start and end of growing season is proxy for the leaf-flush and leaf-fall, respectively. The results of satellite-based analysis include uncertainty due to heterogeneity of vegetation within an area per pixel in satellite remote-sensing data, and cloud contamination and atmospheric noise. The timing of snowmelting, leaf-flush, leaf-fall, and snow covering was affected by the latitudinal gradient in Alaska (Fig. 21.10, Sugiura et al. 2013; Kobayashi et al. 2016). To obtain ground-truth of this characteristic, phenological observations using time-lapse digital cameras installed along the Alaskan highway are useful (Sugiura et al. 2013; Kobayashi et al. 2016). Further field studies at multiple points where time-lapse digital cameras have been installed should be conducted to obtain ground-truth of LAI estimation. In this case, we should pay heed to the relationship among canopy-openness, LAIu, and LAIo in each study site.

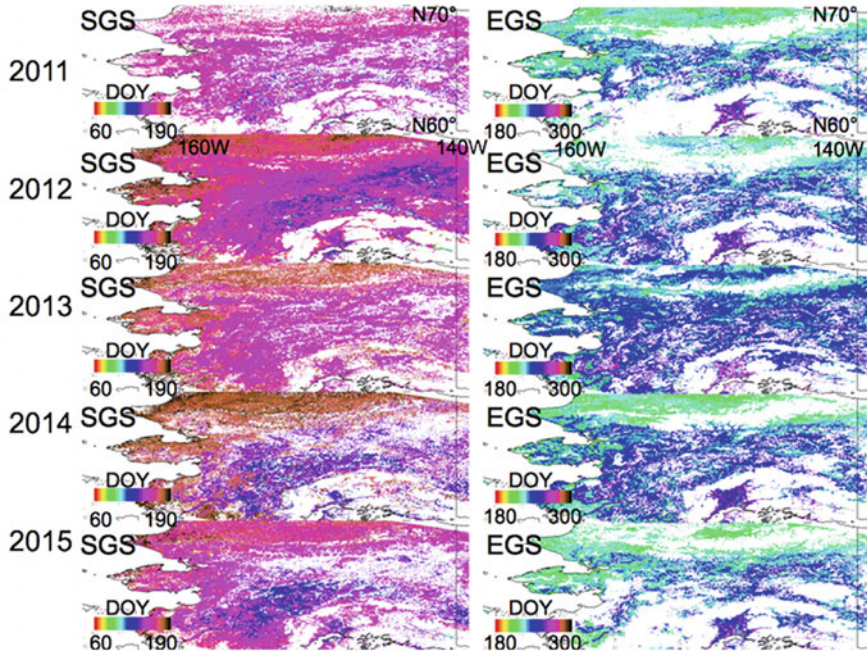
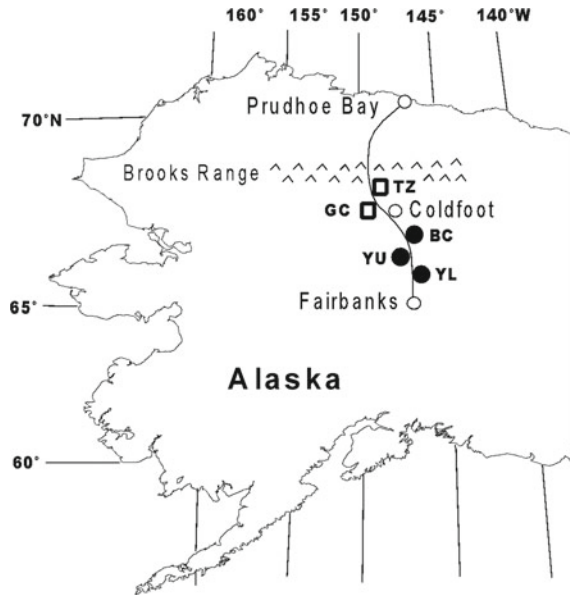


**Fig. 21.10** Spatio-temporal distribution of the timing of start (SGS) and end of growing season (EGS) from 2011 to 2015 in Alaska analyzed by time-series in daily MODIS Terra/Aqua satellites-observed green-red vegetation index (GRVI). The timing of SGS and EGS was defined as the first day on which GRVI was more than or equal to zero in spring and the first day on which it was less than zero in autumn, respectively (Nagai et al. 2015). White shows pixels where we could not evaluate the timing of SGS and EGS or evergreen forests

#### 21.2.4 Spatial Distribution of Winter and Spring Soil CO<sub>2</sub> Emission

Soil CO<sub>2</sub> efflux, produced by decomposition of soil organic carbon and roots, signifies the second largest terrestrial carbon source on both time and space scales (Schlesinger and Andrews 2000). The magnitude of soil CO<sub>2</sub> efflux may depend on the timing of snow disappearance and the snow cover duration (Sturm et al. 2005). During the seasonally snow-covered period, winter CO<sub>2</sub> measurements in boreal forests (Winston et al. 1997; Kim et al. 2007, 2013; Kim 2014), account for 10–30% of the variability in annual carbon emissions. On the other hand, it is difficult to determine the timing of snow disappearance in the early spring season, due to fast snowmelt, including change of  $-0.94$  day year<sup>-1</sup> over 14 years in terrestrial Pan-Arctic drainage basin and Alaska, according to microwave remote sensing (McDonald et al. 2004). Such shifts may cause decrease in subarctic CO<sub>2</sub> efflux in both winter and the growth season (Sturm et al. 2005), resulting from changes in solar radiation (e.g., energy exchange) (Eugster et al. 2000). It is important,

**Fig. 21.11** Site locations along the trans-Alaska pipeline, during winter and spring seasons of 2010–2012. Solid circles are black spruce forest sites and open squares are white spruce forest sites (revised by Kim 2014)



therefore, to understand and qualify soil carbon balance—whether it shows the acceleration of photosynthesis and respiration or their decline—as it controls the terrestrial carbon budget in response to a changing climate in northern high latitudes.

Quantification of winter carbon emission is extremely significant in determining annual carbon budget. Using a dynamic chamber system, soil CO<sub>2</sub> efflux was measured at five boreal forest sites, two in white spruce and three in black spruce forest along the Dalton Highway, over a distance of 700 km, during the winter and spring seasons of 2010–2012 (Fig. 21.11).

Sites were classified as two ecotypes in interior Alaska: white spruce forest (TZ and GC) and black spruce forest (BC, YU, and YL), depending on dominant vegetation, local weather, and permafrost. The boreal forest extends across the lowlands and uplands of the Tanana-Yukon flats, comprising white and black spruce and deciduous forests (Raynolds et al. 2006; Kim et al. 2013; Kim 2014).

Snowpack began to melt in areas surrounding boreal forest trees during early May (Fig. 21.12). The melt process around trees proceeds as follows (Kojima 2001): (1) tree trunks directly absorb strong solar energy (e.g., short wavelength) from the sun, due to lower reflectance of trees; (2) temperatures of tree stems increase; (3) warmed stems emit radiation as long wavelengths during nighttime; (4) snow surrounding tree trunks melts in concentric circles (e.g., ablation rings) around stems (Winston et al. 1997); (5) dents surrounding stems and tussock open in round and oval shapes; (6) dents extend to the ground; (7) soil around stems expose; (8) ground is exposed as the temperature rises; and finally (9) larger dents from melting snow are completed down to the bases of stems. For the Canadian

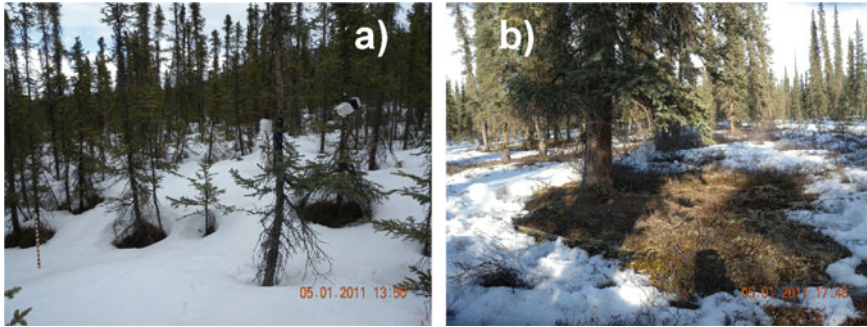


**Fig. 21.12** Site views in **a** black spruce forest site (BC, YU, and YL), **b** white spruce sites (GC and TZ) during spring of 2011. Exposed soils were found in surrounding truck well due to fast snowmelt by shortwave radiation for nighttime (Photos by Y. Kim)

boreal forest, Winston et al. 1997 and Kim 2014 explained that an important mechanism of CO<sub>2</sub> transport through the forest snowpack was by macro-channels along trunks and stems, as previously described regarding snow-melting mechanisms near the tree stem. Soil CO<sub>2</sub> efflux was measured in the exposed and snow-covered soils of boreal forests during spring.

Using a portable chamber, soil CO<sub>2</sub> efflux measurements were conducted during snow-covered and snow-melting periods to minimize artificial effects, as described in Kim et al. (2013). Nine chamber bases were inserted into the soils of boreal forest sites during spring. To prevent contamination and disturbance, chamber bases were not used at boreal sites during snow-covered periods, due to soft snow surface (Kim et al. 2007, 2013; Kim 2014).

Flux measurement times were at 5–10 min intervals, depending on local weather and soil surface conditions, and efflux was calculated using the following equation, as described by Kim et al. (2007, 2013):

$$F_{\text{CO}_2} = \rho_a \times (\Delta C / \Delta t) \times (V / A) \quad (21.1)$$

where  $\rho_a$  is the molar density of dry air (mol m<sup>-3</sup>),  $\Delta C$  (ppmv) is the change in CO<sub>2</sub> concentration during the measurement period ( $\Delta t$ , 5–10 min),  $V$  is chamber volume, and  $A$  is surface area (cross section = 0.28 m<sup>2</sup>). The pump was maintained at a flow rate of 1.0 L min<sup>-1</sup> to avoid underestimation or overestimation of carbon flux from the occurrence of under- and over-pressurization between the inside and outside of the chambers (Savage and Davidson 2003). The height of each chamber was also measured alongside the chamber to allow efflux calculation.

To estimate the response from temperature dependence on soil CO<sub>2</sub> efflux, the relationship was plotted, showing exponential curves on soil temperature at 5 cm depth from the equation:

$$\text{CO}_2 \text{ efflux} = \beta_0 \times e^{\beta_1 \times T} \quad (21.2)$$

where  $\text{CO}_2 \text{ efflux}$  is the measured *soil*  $\text{CO}_2 \text{ efflux}$  ( $\text{g C m}^{-2} \text{ day}^{-1}$ ),  $T$  is soil temperature ( $^{\circ}\text{C}$ ), and  $\beta_0$  and  $\beta_1$  are constants. This exponential relationship is commonly used to represent soil carbon flux as a function of temperature (Davidson et al. 1998; Xu and Qi 2001; Davidson and Janssens 2006; Rayment and Jarvis 2000; Kim et al. 2007, 2013; Kim 2014).  $Q_{10}$  temperature coefficient values were calculated as in Davidson et al. (1998), Kim et al. (2013), and Kim (2014):

$$Q_{10} = e^{\beta_1 \times 10} \quad (21.3)$$

where  $Q_{10}$  is a measure of the change in reaction rate at intervals of  $10^{\circ}\text{C}$  and is based on Van't Hoff's empirical rule that a rate increase of two to three times occurs for every  $10^{\circ}\text{C}$  rise in temperature (Lloyd and Taylor 1994).

During the winter season,  $\text{CO}_2$  concentration gradients in snowpack between trees and near tree wells were 2.52–4.78 and 0.93–1.20  $\text{ppm cm}^{-1}$ , measured using a stainless steel-made probe (0.4 cm OD; 0.2 cm ID; 80 cm long) with connecting tubing, tri-way stopcock, and syringe at sub-surface and bottom snowpack depths, respectively. This suggests that a lower  $\text{CO}_2$  gradient near the tree trunk results in faster  $\text{CO}_2$  transport from the soil through snowpack to the atmosphere than through snowpack between trees. This demonstrates that the air–snow–soil interface surrounding the tree trunk is much thinner than in forest opening areas.

During spring, average  $\text{CO}_2$  effluxes are much higher in exposed than snow-covered soils. Because the snow-disappearance date in 2011 was approximately 10–17 days earlier than in both 2010 and 2012, based on four-hour time-lapse camera measurements, and spring  $\text{CO}_2$  efflux in exposed soils in 2011 was at least tenfold higher than in snow-covered soils.

Three-year average spring  $\text{CO}_2$  effluxes are completely different in four directions within the white spruce forest (Fig. 21.13a and b). The magnitude of snow disappearance depends on solar radiation and the strength of long wavelengths from the tree trunk at nighttime during the spring. The much wider exposed area showed south > east  $\cong$  west  $\gg$  north, in turn, from trunks in the white spruce forest. Average diameter at breast height (DBH;  $18 \pm 4.5$  cm) for white spruce is much thicker than black spruce (DBH  $5.8 \pm 3.2$  cm), suggesting that the difference in radiation uptake and heat emission capacity between both forests resulted in that of dent size, as shown in Fig. 21.13a and b. This feature is related to the differences in exposed extent and soil  $\text{CO}_2$  production within boreal forest sites.

Higher  $Q_{10}$  values for the winter and spring seasons were found within boreal white and black spruce forests, and tundra sites across the Dalton Highway, relative to  $Q_{10}$  values of 2.1–18 in the growing season (Kim et al. 2013). This result suggests the exponential growth of microbes (e.g., snow molds) results from warming of soils below snowpack from  $-3$  to  $0^{\circ}\text{C}$  produced higher  $\text{CO}_2$  in a subalpine forest in the Colorado Front Range (Monson et al., Monson et al. 2006a, b; Schmidt et al. 2007). Monson et al. (2006a, b) demonstrated that soil microbes'

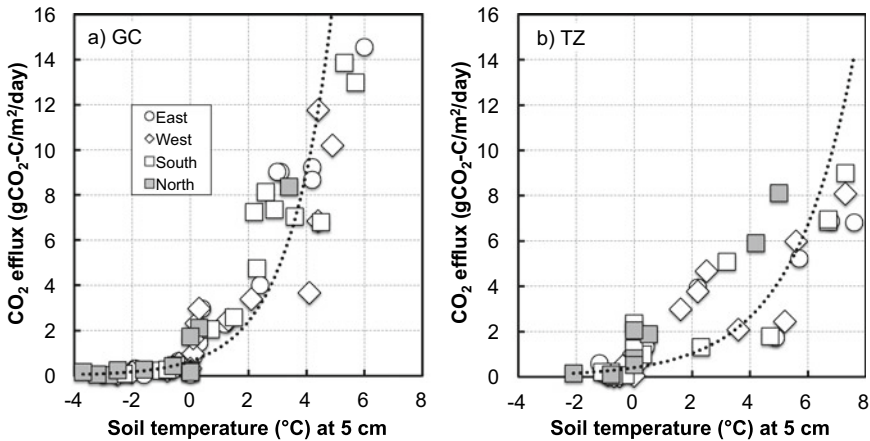


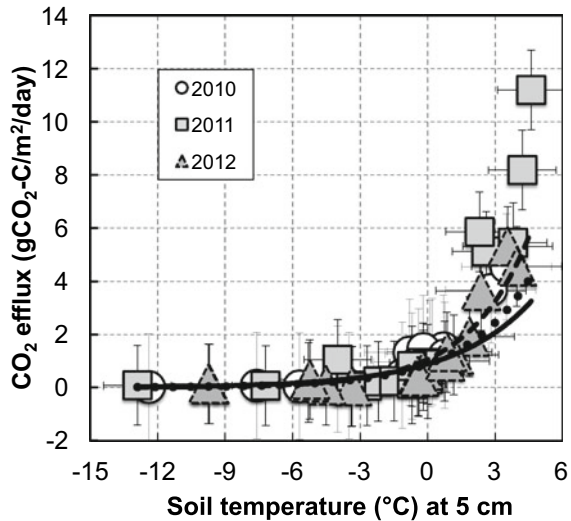
**Fig. 21.13** Responses of spring  $\text{CO}_2$  efflux on soil temperature at 5 cm below the surface measured in four-direction from the stem of white spruce in **a** GC and **b** TZ sites during the spring. The dotted curves denote the 3-year exponential relationship between spring  $\text{CO}_2$  efflux and soil temperature

beneath-snow  $\text{CO}_2$  efflux response (e.g.,  $Q_{10}$  value: 105 to  $1.25 \times 10^6$ ) corresponded to a narrower range of soil temperature ( $-1.0$  to  $0.0$  °C). Further, the drastic increase in  $\text{CO}_2$  efflux was induced by a strong response from beneath-snow microbes, with a much higher dependence from microbial biomass upon an increase in soil temperature in the late winter and early spring seasons (Schmidt et al. 2007).

The response of spring  $\text{CO}_2$  efflux to soil temperature at 5 cm below the soil surface at all sites during the spring seasons of 2010–2012 is shown in Fig. 21.14. Three-year spring  $\text{CO}_2$  efflux shows spatial distribution across  $66$ – $70^\circ\text{N}$ , along the Dalton Highway, with latitudinal distribution of soil temperature at 5 cm. Higher efflux was seen in white spruce forest sites, at  $>5 \text{ g C m}^{-2} \text{ day}^{-1}$ , reflecting an ablation ring effect. Winston et al. (1997) further suggested that soil  $\text{CO}_2$  efflux from a tree well was tenfold higher than that for forest openings. There is thus a clear difference in spring  $\text{CO}_2$  efflux between a tree trunk in exposed soils and a forest opening in seasonally snow-covered soils.

Growing season  $\text{CO}_2$  efflux measurements were conducted at each site from August to September of 2010. However, as efflux could not be measured during 2011 and 2012, due to rainy and cold weather conditions in the late fall season (i.e., late September to early October), calculation of seasonal emissions has used data observed in 2010 and by Kim et al. (2013). Further, the contribution of average three-year winter and spring  $\text{CO}_2$  emissions to the atmosphere corresponds to roughly 14–22% for tundra and 9–24% for boreal forest sites, of the total annual carbon respired. Winter  $\text{CO}_2$  contributions to annual carbon emissions within tundra, alpine, and boreal forest ecosystems represent from 17% for Alaskan tundra (Fahnestock et al. 1998) to  $>25\%$  for alpine and subalpine regions (Sommerfeld

**Fig. 21.14** Responses of spring CO<sub>2</sub> efflux on soil temperature at 5 cm below the surface in whole sites during the spring seasons of 2010 and 2012. The dashed, dotted, and solid curves denote 2010, 2011, and 2012, respectively



et al. 1993), suggesting that the results of this study are comparable with others. However, spring CO<sub>2</sub> contributions from the boreal forest reached to almost 50% of growing season carbon emissions, demonstrating the strong tree-well effect (Winston et al. 1997) of the boreal forest (Kim et al. 2007, 2013; Kim 2014). Spring carbon contributions, like growing season CO<sub>2</sub> emissions, were sensitive to subtle changes in the onset of spring and snowpack covering duration.

### 21.2.5 Successional Changes in CO<sub>2</sub> and Energy Balance After Forest Fires

Vegetation in boreal forest ecosystems is a net carbon sink of 0.54 Gt year<sup>-1</sup> and that the soil of boreal forest and peatlands represent a net carbon sink of 0.70 Gt year<sup>-1</sup> (Apps et al. 1993). Further, boreal forest ecosystems are particularly subject to cyclic disturbance by forest fire (e.g., wildfire). The shift of the boreal forest from a net sink to a net source of atmospheric carbon, then, will likely originate from two sources, both anthropogenic in their origin: (1) likely increases in deforestation activities in the boreal forest; and (2) increases in disturbances in the region due to climate change, such as fire, insect outbreak, and pathogens (Kasischke and Stocks 2000). Recent studies in the boreal black spruce forest biomes of Alaska have shown that changes in the local energy balance may result in post-fire biogenic emissions of carbon that equal or exceed the amount of carbon dioxide (CO<sub>2</sub>) released during forest fire (Richter et al. 2000; Hicke et al. 2003; Kim and Tanaka 2003; O'Neill et al. 2003, 2006), potentially shifting large areas of the landscape from net CO<sub>2</sub> sinks to net CO<sub>2</sub> sources. This is to say that, immediately following forest fire, the fixation of CO<sub>2</sub> by vegetation such as juniper haircap moss is

minimal to non-existent, while rates of decomposition may be stimulated as a result of warmer soil temperature and changes in soil drainage (Richter et al. 2000; Kim and Tanaka 2003; O'Neill et al. 2003).

Juniper haircap moss (*Polytrichum juniperinum*) is typically a pioneer species—the first groundlayer species to establish after fire—and is characteristically found on burned mineral soils and other charred substrates (Fryer 2008). Also, juniper haircap moss, as a fire-follower, may actually survive fire, and it shows a strong ability to colonize newly burned areas, due to the penetration of its rhizoids into mineral soil (Skutch 1929; Schimmel and Granstrom 1996; Ruokolainen and Salo 2006). This adaptation allows juniper haircap moss to survive some surface fires. The species is well adapted to large fluctuations in summer temperature, higher light levels, and the low humidity levels typical of recently burned soils (O'Neill et al. 2006). Under optimal moisture conditions, mosses contributed between 10 and 55% of total soil respiration after forest fire, with highest contributions from early successional moss species (*Ceratodon purpureus* and *P. juniperinum*) (O'Neill et al. 2006). Just after fire, soil respiration decreased by, at most, 50%; however, microbial respiration estimated after the fire was almost three times as high as calculated respiration before the fire (Kim and Tanaka 2003). This indicates that the post-fire condition may stimulate microbial respiration, on account of higher nutrients and substrates in remnant soils and enhanced soil temperature (Kim and Tanaka 2003). It is important, then, to understand carbon dynamics in juniper haircap moss regimes after forest fire.

Our study site began as a mature black spruce (*Picea mariana*) forest before the fire of 2004, located within the Poker Flat Research Range (PFRR) of the University of Alaska Fairbanks (UAF) in interior Alaska. The forest fire ignited due to lightning in mid-June of 2004 and continued until early August 2004. We subsequently measured CO<sub>2</sub> exchange rates and microbial respiration using an automated chamber system over August–October 2009 at this severely burned site (65° 08'N, 147° 26'W, 491 masl). The site was selected according to the criterion that no vegetation other than juniper haircap moss regimes occurs within a 10-m radius. A single chamber system set, consisting of transparent and opaque chambers, was installed on the moss regime for the estimation of CO<sub>2</sub> exchange rates. Two sets were prepared over a no-plants regime for microbial respiration rate (MR). The remaining soil organic layer was 2 cm deep, underlain by sandy silt with gravel (Iwata et al. 2011). We assumed that the dead roots of the severely burned black spruce were not yet decomposed and contributed to soil respiration, due to their completely charred roots. This suggests that the microbial respiration rates produced in burned black spruce forest soil are presumably constant. Most of the burned black spruce trees remained snag, and some were logged due to snowfall after winter. The fractional area covered by vegetation at a nearby area with similar burn conditions was 26% in August 2005; this increased to 85% in August 2008, four years after the fire (Tsuyuzaki et al. 2009). Major vegetation consisted of paper birch (*Betula papyrifera*), quaking aspen (*Populus tremuloides*), Labrador tea (*Ledum palustre*), bog blueberry (*Vaccinium uliginosum*), sedge (*Eriophorum scheuchzeri*), fireweed (*Epilobium angustifolium*), and juniper haircap moss

(*Polytrichum juniperinum*). As juniper haircap moss is typically among the first ground-layer species to establish after fire (Foster 1985), our study focuses on the carbon dynamics of juniper haircap moss during the fall season.

CO<sub>2</sub> exchange rates (i.e., NPP: net primary productivity, Re: ecosystem respiration, and GPP: gross primary productivity) were measured in this instance of burned black spruce forest moss. NPP and Re were measured using light and dark chambers; NPP may be calculated using the following equation and NEP (net ecosystem productivity) using Eq. (21.5).

$$NPP = Re - GPP \quad (21.4)$$

$$NEP = NPP - MR \quad (21.5)$$

where  $MR$  is microbial respiration (g CO<sub>2</sub> m<sup>-2</sup> h<sup>-1</sup>) measured in a no-vegetation condition of the burned black spruce forest.

A reference value of  $R_{10}$  (MR normalized to a temperature of 10 °C) was then calculated as:

$$R_{10} = R_i \cdot Q_{10}^{[(10-T)/10]}, \quad (21.6)$$

where  $R_i$  is the measured MR (g CO<sub>2</sub> m<sup>-2</sup> h<sup>-1</sup>) at  $T$  temperatures in air (°C). Using the calculated values of  $Q_{10}$  and  $R_{10}$ , MR was simulated on the basis of the measured air temperature. Simulated MR values,  $R_i$  (g CO<sub>2</sub> m<sup>-2</sup> h<sup>-1</sup>), were calculated as:

$$R_i = R_{10} / Q_{10}^{[(10-T)/10]}, \quad (21.7)$$

Using the automated chamber system, we measured CO<sub>2</sub> exchange rates of juniper haircap moss and soil—primarily microbial (e.g., heterotrophic)—respiration, within the burned black spruce forest. Microbial respiration can only be estimated in the burned forest, as root activity ceased after the wildfire. Two kinds (transparent and opaque) of chambers were assembled in *P. juniperinum* moss in order to measure CO<sub>2</sub> exchange rates, the rest were placed in no-vegetation ground of the burned black spruce forest to capture microbial respiration.

### 21.2.6 Seasonal Variation in CO<sub>2</sub> Exchange Rate in Juniper Haircap Moss

CO<sub>2</sub> exchange rates, such as NPP by light chamber and Re by dark chamber, were measured in juniper haircap moss of burned black spruce forest during the fall season of 2009. Mean NPP and Re were  $-0.01 \pm 0.33$  and  $0.31 \pm 0.19$  g CO<sub>2</sub> m<sup>-2</sup> h<sup>-1</sup>, respectively. Mean GPP was calculated using Eq. (21.1), yielding  $0.31 \pm 0.41$  g CO<sub>2</sub> m<sup>-2</sup> h<sup>-1</sup>. In no-vegetation soil of the burned black spruce

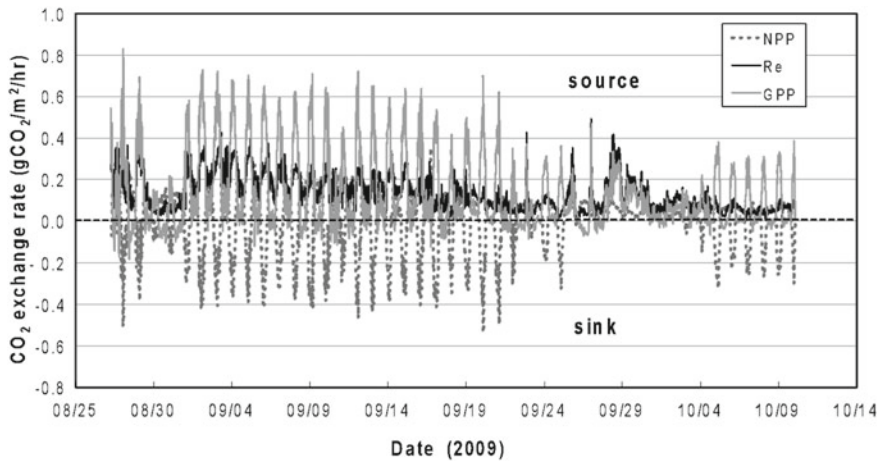


**Fig. 21.15** Seasonal variations of NPP (dashed line), Re (solid line), and GPP (thin solid line) in the haircap moss of burned black spruce forest. Source, that carbon dioxide emits to the atmosphere, denotes over the zero as Re and GPP, and sink, that the moss photosynthesizes, shows below the zero, as NPP (Kim et al. 2014)

forest, mean microbial respiration from light and dark chambers showed  $0.21 \pm 0.10 \text{ g CO}_2 \text{ m}^{-2} \text{ h}^{-1}$ , and  $0.29 \pm 0.11 \text{ g CO}_2 \text{ m}^{-2} \text{ h}^{-1}$ , respectively—not a significant difference at a 95% confidence level. This suggests that the microbial respiration of the burned plot can be considered constant within 50% of CV. Mean NEP was calculated using Eq. (21.5), yielding  $-0.28 \pm 0.38 \text{ g CO}_2 \text{ m}^{-2} \text{ h}^{-1}$  and a range of  $-1.65$  to  $0.44 \text{ g CO}_2 \text{ m}^{-2} \text{ h}^{-1}$ , indicating juniper haircap moss as a net sink in the five-year-old burned black spruce forest (Fig. 21.15).

Simulated microbial respiration was calculated using Eq. (21.7), yielding mean simulated MR (L and D) of  $0.23 \pm 0.14$  (CV: 57%) and  $0.32 \pm 0.16$  (CV: 48%)  $\text{g CO}_2 \text{ m}^{-2} \text{ h}^{-1}$ , respectively. Based on a one-way ANOVA at a 95% confidence level, these values show no significant differences in measured MR (L and D). Litvak et al. (2003) and O'Neill et al. (2003) estimated NEP and C source-sink dynamics for various stands using a modified mass balance model of C storage that allowed both decomposition and NPP to vary over the fire cycle. Mean daily NEP calculated in our study was  $0.28 \pm 0.16$  (CV: 58%)  $\text{g CO}_2 \text{ m}^{-2} \text{ h}^{-1}$  in the juniper haircap moss of burned black spruce forest. NPP of *P. juniperinum* moss ranged from  $0.25 \text{ Mg C ha}^{-1}$ , as a source of atmospheric  $\text{CO}_2$ , to  $0.56 \text{ Mg C ha}^{-1}$ , as a net sink during the 45-day fall period. Using Eq. (21.5), mean NEP of *P. juniperinum* moss was  $0.49 \pm 0.28 \text{ Mg C ha}^{-1}$ , after 5-year-old forest fire. O'Neill et al. (2006) reported that total inputs to the soil system (NPP) were estimated to increase from 0.0 to 0.8–1.5  $\text{Mg C ha}^{-1}$  during the first 100 years after fire. The difference between modeled NPP and decomposition suggested that these soils were a net C source for 7–14.5 years after fire and a net sink of 0.3–0.6  $\text{Mg C ha}^{-1}$  over the remaining (140) years (O'Neill et al. 2006). These trends are generally consistent

with those of Bond-Lamberty et al. (2004) for a black spruce fire chronosequence in Manitoba, Canada, in which NEP showed a small post-fire net C loss followed by a long period of positive accumulation with a maximum NEP of  $1.1 \text{ Mg C ha}^{-1}$  (71 years post-fire). However, our NEP finding suggests that *P. juniperinum* moss plays a net sink role within a 5-year burned black spruce forest during fall season. To estimate ecosystem NEP after a fire during the growing season, additional study is required to monitor  $\text{CO}_2$  exchange rates in other ground plants such as shrubs and bryophyte within the same site.

Based on the relationship between measured microbial respiration and simulated microbial respiration, normalized to a temperature of  $10^\circ\text{C}$  by Eq. (21.7) using light and dark chambers in black spruce forest after fire, we calculated seasonal simulated MR using Eq. (21.7), based on daily air temperature during the growing season (May to October) of 2009 (Fig. 21.16). During the 45-day observation period, the cumulative measured MR of  $11.2 \text{ g CO}_2 \text{ m}^{-2}$  is similar to  $10.8 \text{ g CO}_2 \text{ m}^{-2}$  of simulated MR, suggesting no significant difference between both at a 95% confidence level, and that air temperature as a significant factor in regulating microbial respiration in the burned black spruce forest of interior Alaska, five years after forest fire.

Forest fires return old-growth forests to young productive ecosystems. In boreal Alaska and Canada, chronosequence studies showed the successional trajectory of  $\text{CO}_2$  budget after forest fires (Amiro et al. 2010; Goulden et al. 2010). Just after the fire, fire scars acted as net annual  $\text{CO}_2$  source of approximately  $200 \text{ g C m}^{-2} \text{ year}^{-1}$  (Goulden et al. 2010). Due to vegetation recovery, carbon source decreased quickly in second year after the fire, but still acted as small  $\text{CO}_2$  source for 10–20 years. This early successional stage is mostly dominated by grasses, shrubs, and young tree saplings. Then, deciduous trees (e.g., *Populus tremuloides* and *Betula papyrifera*) become dominant and the ecosystem turn to strong  $\text{CO}_2$  sink. Through this

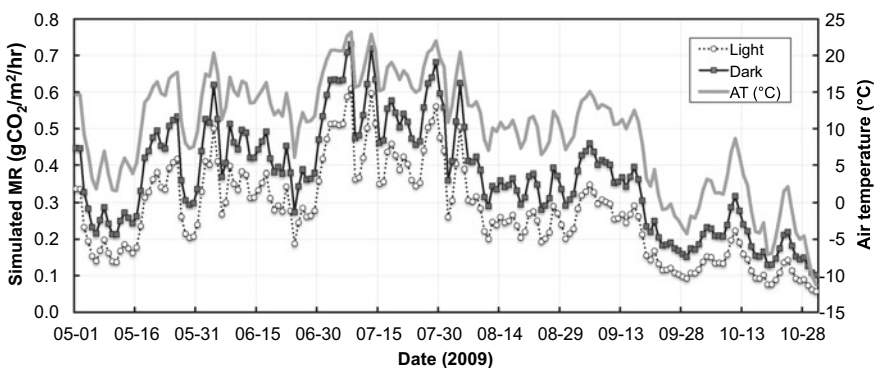


**Fig. 21.16** Temporal variations of microbial respiration from light (dotted line) and dark (solid line) chambers, and air temperature at 2.3 m (grey line) during the growing season (May to October) of 2009, based on the estimation of the Eq. (21.7)

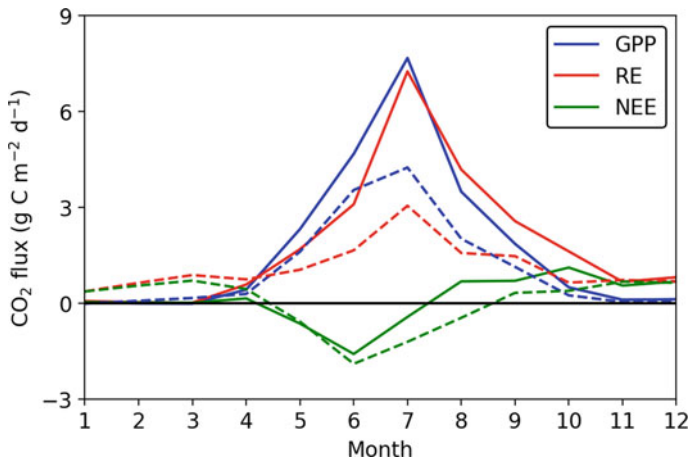


**Fig. 21.17** Seasonal variations of CO<sub>2</sub> fluxes at a mature black spruce forest (solid line) and a burned forest five years after the fire (dashed line) at interior Alaska (after Iwata et al. 2011)

productive stage, ecosystems accumulate carbon in vegetation, litter, and soils, resulting in slowly succession to mature stage where evergreen needle leaf trees (e.g., *Picea mariana*) dominates. In the mature to old growth stage, CO<sub>2</sub> sink of the ecosystems slowly dampened due to increases in autotrophic and heterotrophic respiration. Since mature and old growth forests are susceptible to fires due to much of fuel loads, fires return these forests to young forest, and emit almost all carbon accumulated in the succession into the atmosphere. Consequently, boreal forests are presumed to be a net CO<sub>2</sub> neutral throughout this fire cycle.

Eddy covariance measurements in interior Alaska showed the different carbon budget among early succession after a forest fire and a mature black spruce forest, in terms of magnitude of fluxes, and the annual budget (Fig. 21.17). Magnitude of the annual GPP was approximately 40% smaller in early succession (five years after a forest fire) than a mature forest. Despite of the smaller GPP, CO<sub>2</sub> sink during May to August was greater in the early succession (approximately 500 g C m<sup>-2</sup> year<sup>-1</sup>) than the mature forest (approximately 240 g C m<sup>-2</sup> year<sup>-1</sup>). This was because the heterotrophic respiration was smaller in the early succession than the mature forest (Iwata et al. 2011). In the early succession, soil and litter carbon were burned in the fire, and were not accumulated. Thus, vegetation recovery was the major driver of the carbon balance in the stage of early succession. In contrast, carbon accumulation and associated increase in respiration was the driver of the carbon balance in the mature stage (Amiro et al. 2010; Goulden et al. 2010).

Effects of forest fires were also seen in satellite remote sensing at the regional scale. An upscaled CO<sub>2</sub> fluxes using satellite remote sensing showed patchy increase or decrease trends in recently burned areas over Alaska (Ueyama et al. 2013). The disturbance effects were seen early successions until approximately

20 years after fires by the satellite remote sensing. Areas suffered from recent fires showed negative trends of GPP, and RE, and positive trends of NEE during the period from 2000 to 2011, due to a sudden decline of productivity. In contrast, areas that suffered from fires more than 10–20 years ago showed positive trends of GPP, and RE, and negative trends of NEE due to a vegetation recovery. Increasing trends in GPP were generally seen until approximately 60 years after fires, and then showed negative or insignificant trends. Consequently, forest fires strongly affect spatial distributions in CO<sub>2</sub> balance of boreal forests in interior Alaska.

Boreal forest fire changes the surface albedo. Just after forest fires, summer albedo decreases due to an exposure of black charcoal (Chambers and Chapin 2003). But, this is not necessarily the case, where summer albedo just after the fire was reported to be greater in fire scar than coniferous forest (Liu and Randerson 2008). Based on a satellite observation of surface albedo, summer albedo increased  $0.135 \pm 0.006$  by dominating shrubs and young trees in stands 20–35 years, which was greater than deciduous or coniferous forests (Lyons et al. 2008). Even summer albedo slowly decreased at stands 40–50 years after fires, the albedo was still higher than coniferous forests (Lyons et al. 2008). Winter albedo in fires scars was higher than the coniferous forest until near 50 years after fire (Lyons et al. 2008).

Change in surface energy balance associated with the albedo change cools the regional climate (Randerson et al. 2006). The increases in albedo increase net shortwave radiation, and thus decrease net radiation (Euskirchen et al. 2010; Ueyama et al. 2014). Albedo-induced change in radiative forcing was estimated as  $-4.2 \text{ W m}^{-2}$ , which was greater than changes by other fire-induced radiative forcing, such as greenhouse gas budget, ozone, black carbon deposition, and aerosols (Randerson et al. 2006). Consequently, boreal forest fires were estimated to act as a net surface cooling due to decreasing net radiative forcing by  $-2.3 \text{ W m}^{-2}$  over an 80-year fire cycle (Randerson et al. 2006).

Forest fire significantly decreased soil CO<sub>2</sub> efflux by a range of 22–50% compared to before fire in the black spruce forest (Kim and Tanaka 2003). Kasischke (2000) and Richter et al. (2000) found that the fire decreased total soil respiration rate by 33–59 and 44–58%, respectively. The differences in rate decreased depend on fire severity, indicating that fire typically consumes between 20 and 90% of the organic soil layer, including any living roots present in this layer (Kasischke et al. 2000a, b). Forest fire in the study site was extremely severe (Iwata et al. 2011). We used mean soil respiration ( $0.22 \pm 0.09$  (CV: 40%)  $\text{g CO}_2 \text{ m}^{-2} \text{ h}^{-1}$ , unpublished data) for the partition of root and heterotrophic respiration rates, which is the sum of plant root respiration and microbial respiration, in mature black spruce forest during the fall season of August 27 to October 5, 2009. Schlentner and Can Cleve (1985) estimated that approximately 20% of soil respiration in mature black spruce forest was derived from microbial respiration, and the remainder was from plant root respiration. Using the partition and mean soil respiration measured in mature black spruce forest, microbial respiration can be calculated as  $0.043 \pm 0.017 \text{ g CO}_2 \text{ m}^{-2} \text{ h}^{-1}$ , possibly solely from microbial respiration from the soil. This is almost six-fold higher than the mean microbial respiration estimated by this study, using the factor of Schlentner and Van Cleve (1985). This finding

indicates that the post-fire condition may greatly stimulate microbial respiration, due to higher nutrients and substrates in remnant soil after forest fire. Furthermore, Kasischke (2000) and Van Cleve et al. (1983) demonstrated that the forest floor temperature for boreal black spruce forests underlain by permafrost remains warmer than in unburned black spruce forests for at least 20–30 years after fire.

According to the proportionality of Schlentner and Van Cleve (1985), mean microbial respiration in 5-year-old burned black spruce forest is estimated to be  $0.27 \text{ g CO}_2 \text{ m}^{-2} \text{ h}^{-1}$ . Of this,  $0.23 \text{ g CO}_2 \text{ m}^{-2} \text{ h}^{-1}$  is attributed to post-fire stimulation of microbial decomposition after the fire. For the 45-day fall season observation period of 2009, microbial respiration may be stimulated by as much as  $0.40 \pm 0.23 \text{ Mg C ha}^{-1}$  in burned black spruce forest, compared with  $0.15 \text{ Mg C ha}^{-1}$  in one year,  $0.38 \text{ Mg C ha}^{-1}$  in seven years, and  $0.40 \text{ Mg C ha}^{-1}$  in ten years after severe forest fire during the fall season (Richter et al. 2000), and with  $0.33 \text{ Mg C ha}^{-1}$  in one year,  $0.58 \text{ Mg C ha}^{-1}$  in seven years, and  $0.45 \text{ Mg C ha}^{-1}$  in ten years after forest fire during the fall season (O'Neill et al. 2006). With the successional vegetation stage, atmospheric  $\text{CO}_2$  is steadily taken up to ground vegetation (e.g., post-fire frontier species—juniper haircap moss and fireweed, sedge, Labrador, bog blueberry, paper birch, quaking aspen) after a fire. However, soil-originated  $\text{CO}_2$  emission to the atmosphere (e.g., primarily microbial respiration and plant respiration) is much more than atmospheric carbon fixation by vegetation in burned black spruce forest. This suggests that the post-fire black spruce forest plays a prolonged, crucial role as a source of atmospheric  $\text{CO}_2$  after forest fire, and that fire severity also yields long-term patterns of post-fire floor temperature and moisture in boreal forest by way of drastic changes in albedo (Richter et al. 2000; O'Neill et al. 2006). Occasionally, we found greater differences in the magnitude of post-fire carbon emission according to research sites, at which the difference in emissions results from a magnitude of fire severity that is closely related to successional chronosequence, soil temperature, and soil moisture (Van Cleve et al. 1983; Kasischke 2000; Kasischke et al. 2000a, b).

In order to understand floor-level carbon dynamics in dominant ground plants of burned black spruce forest, additional study was conducted in order to monitor  $\text{CO}_2$  exchange rates and microbial respiration, using an improved automated chamber system during the growing season, and an FD (forced diffusion) soil  $\text{CO}_2$  efflux method during the winter season (Risk et al. 2011). Figure 21.18 showed temporal variations of microbial respiration, air temperature, and soil temperature in burned black spruce forest soil of the Poker Flat Research Range (PFRR), from August 2015 to October 2016. Their data provide the estimation of carbon exchange rates on juniper haircap moss and young black spruce through the ecologically successional stages after 2004 forest fire.

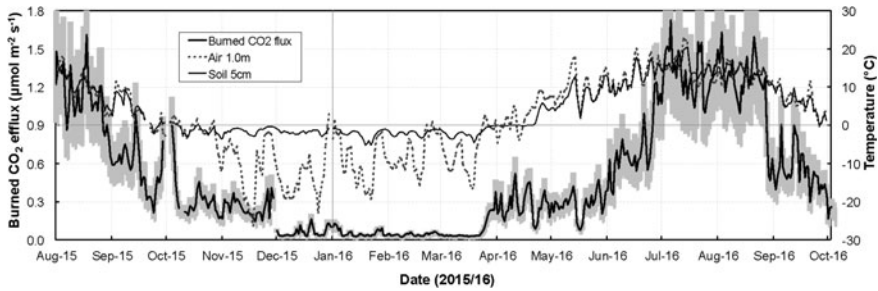


**Fig. 21.18** Temporal variations of microbial respiration with FD chamber (thick solid line), air temperature at 1.0 m above soil surface (dotted line), and soil temperature at 5 cm depth under the surface in 2004 burned black spruce forest soil of the Poker Flat Research Range (PFRR) from August 2015 to October 2015 (unpublished data)

### 21.3 Summary

Boreal forest is a significantly net carbon sink reservoir of  $0.54 \text{ Gt C year}^{-1}$ , whereas tundra ecosystems are currently a net carbon source of  $0.17 \text{ Gt C year}^{-1}$  (Apps et al. 1993). However, boreal forest may become a net source of carbon, resulting from deforestation activity and increase in the disturbances (e.g., forest fire, insects and pathogens) in response to the warming of Sub-Arctic and Arctic regions. In turn, boreal forest will cause a net release of carbon by anthropogenic and naturally lighting-caused forest fires.

Our main research findings are as follows. First, the aboveground biomass (AGB) mapping in boreal forest is beneficial to evaluate the plant biomass carbon stock, based on in situ field survey and remote-sensing satellite data, in the context of the global biogeochemical cycle in pre- and post-fire landscapes. Second, the responses of climate change, plant phenology, spring green-up, and autumn senescence, as well as timing of snow cover and disappearance in the boreal forest, can be sufficiently investigated with satellite and ground-based observation networks, providing better understanding of the future phenological changes in the successional recovery of disturbed forests after the wildfires. Third, the analysis of time-series of daily satellite-observed vegetation index is useful to detect the spatiotemporal variability of leaf area index (LAI) in the Pan-Arctic terrestrial ecosystems, based on (1) accurate detection of spatiotemporal variability in the timing of snowmelt, leaf-flush, leaf-fall, and snow on date, and (2) collection of ground-truth of LAI, plant phenology, and stratification of forest structure at multiple research stations. Fourth, spring carbon contributions, corresponding to almost 50% of growing season  $\text{CO}_2$  emissions, are sensitive to subtle changes at the onset of snowmelt and snow-cover duration in northern high latitudes along the trans-Alaska pipeline, in response to recent Sub-Arctic and Arctic climate change. Lastly, the under- and overstory vegetation recovery with the successional stages

after wildfires affects the carbon and energy balance in burned boreal forests. Additional study needs to monitor yearlong soil carbon emission in disturbed boreal forest soils for the understanding of floor- and canopy-level carbon dynamics in pre- and post-fire landscapes with eddy covariance tower methods.

**Acknowledgments** This research was supported by a National Research Foundation of Korea Grant from the Korean Government (MSIT; the Ministry of Science and ICT) (NRF-2016M1A5A1901769) (KOPRI-PN20081) (Title: Circum-Arctic Permafrost Environment Change Monitoring, Future Prediction and development Techniques of useful biomaterials (CAPEC Project)). Also, this research was conducted under the JAMSTEC-IARC Collaboration Study (JICS) Project, with funding provided by the Japan Agency for Marine-Earth Science and Technology (JAMSTEC). We are grateful to Dr. Yang Wei (Chiba University) for his valuable comment and for providing a figure. Finally, this manuscript is dedicated to the late Dr. Rikie Suzuki of the JMASTEC, our most treasured colleague.

---

## References

- Alaska Interagency Coordination Center (2018) Alaska fire history from 1940 to present. <https://fire.ak.blm.gov/aicc.php>
- AMAP (2017) Snow, Water, Ice and Permafrost. Summary for Policy-makers. Arctic Monitoring and Assessment Programme (AMAP), Oslo, Norway
- Amiro BD et al (2010) Ecosystem carbon dioxide fluxes after disturbance in forests of North America. *J Geophys Res* 115:G00K92. <https://doi.org/10.1029/2010jg001390>
- Apps MJ, Kurz WA, Luxmoore RJ, Nilsson LO, Sedjo RA, Schmidt R, Simpson LG, Vinson TS (1993) Boreal forests and tundra. *Water Air Soil Pollut* 70:39–53
- Apps MJ, Pries DT (1996) Forest Management and the Global Carbon Cycle, NATO ASI Series, subseries 1, vol. 40, Global Environment Change. Springer-Verlag, Berlin
- Barney RJ, Stocks BJ (1983) Fire frequencies during the suppression period. In: Wein RW, MacLean DA (eds) *The role of fire in northern circumpolar ecosystems*. Wiley, New York, pp 45–61
- Belchansky GI (2004) Arctic ecological research from microwave satellite observations. CRC Press, Boca Raton, FL, USA, p 248
- Billings WD (1997) Challenges for the future: Arctic and alpine ecosystems in a changing world. In: Oechel WC, Callaghan T, Gilmanov T, Holten JI, Maxwell B, Molau U, Svebjörnsson B (eds) *Global change and Arctic terrestrial ecosystems*. Springer, New York, pp 1–18
- Bond-Lamberty B, Wang C, Gower ST (2004) Contribution of root respiration to soil surface CO<sub>2</sub> flux in a boreal black spruce chronosequence. *Tree Physiol* 24:1387–1395
- Buermann W, Parida B, Jung M, MacDonald GM, Tucker CJ, Reichstein M (2014) Recent shift in Eurasian boreal forest greening response may be associated with warmer and drier summers. *Geophys Res Lett* 41:1995–2002
- Chambers SD, Chapin FS III (2003) Fire effects on surface-atmosphere energy exchange in Alaskan black spruce ecosystems: implications for feedbacks to regional climate. *J Geophys Res* 108:8145. <https://doi.org/10.1029/2001JD000530>
- Chapin FS III, Hollingsworth T, Murray DF, Viereck LA, Walker MD (2006) *Floristic diversity and vegetation distribution in the Alaskan boreal forest*. Oxford University Press, New York
- Cronan J, McKenzie D, Olson D (2012) *Fire regimes of the Alaskan boreal forest*. Gen. Tech. Rep. PNW-GTR-XXX. Portland, OR: U.S. Department of Agriculture, Forest Service, Pacific Northwest Research Station
- Crutzen PJ, Andreae MO (1990) Biomass burning in the tropics: impact on atmospheric chemistry and biogeochemical cycles. *Science* 250:1669–1678

- Davidson EA, Belk E, Boone RD (1998) Soil water content and temperature as independent or confounded factors controlling soil respiration in a temperate mixed hardwood forest. *Global Change Biol* 4:217–227
- Davidson EA, Jassens IA (2006) Temperature sensitivity of soil carbon decomposition and feedback to climate change. *Nature* 440:165–173
- Delbart N, Kergoat L, Le Toan T, Lhermitte J, Picard G (2005) Determination of phenological dates in boreal regions using normalized difference water index. *Remote Sens Environ* 97:26–38
- Delbart N, Picard G, Le Toans T, Kergoat L, Quegan S, Woodward I, ... Fedotova V (2008) Spring phenology in boreal Eurasia over a nearly century time scale. *Glob Change Biol* 14:603–614
- Delpierre N, Dufrene E, Soudani K, Ulrich E, Cecchini S, Boe J, Francois C (2009) Modelling interannual and spatial variability of leaf senescence for three deciduous tree species in France. *Agric For Meteorol* 149:938–948
- Dissing D, Verbyla DL (2003) Spatial patterns of lightning strikes in interior Alaska and their relations to elevation and vegetation. *Can J For Res* 33:770–782
- Dyrness CT, Viereck LA, Van Cleve K (1986) Fire in taiga communities of interior Alaska. In: Van Cleve K, Chapin FS, Flanagan PW, Viereck LA. *Forest ecosystems in the Alaskan Taiga*. Springer-Verlag, New York, pp 74–86
- Eschenbach C, Kappen L (1996) Leaf area index determination in an alder forest: a comparison of three methods. *J Exp Bot* 47(302):1457–1462
- Eugster W, Rouse W, Pielke RA, McFadden JP, Baldocchi D, Kittel TF, Chapin FS, Liston GE, Vidale PL, Vaganov E, Chambers S (2000) Land-atmosphere energy exchange in Arctic tundra and boreal forest: available data and feedbacks to climate. *Global Change Biol* 6:84–115
- Euskirchen ES, McGuire AD, Chapin FS III, Rupp TS (2010) The changing efforts of Alaska's boreal forests on the climate system. *Can J For Res* 40:1336–1346
- Euskirchen ES, Bret-Harte MS, Scott GJ, Edgar C, Shaver GR (2012) Seasonal patterns of carbon dioxide and water fluxes in three representative tundra ecosystems in northern Alaska. *Ecosphere* 3(1)
- Fahnestock JT, Jones MH, Brooks PD, Walker DA, Welker JM (1998) Winter and early spring CO<sub>2</sub> efflux from tundra communities of northern Alaska. *J Geophys Res* 103:29023–29027
- Fan S, Gloor M, Mahlman J, Pacala S, Sarmiento J, Takahashi T, Peng T (1998) A large terrestrial carbon sink in North America implied by atmospheric and oceanic carbon dioxide data and models. *Science* 282:442–446
- Foster DR (1985) Vegetation development following fire in *Picea mariana* (black spruce)-*Pleurozium* forests of southeastern Labrador, Canada. *J Ecology* 73:517–534
- Fryer JL (2008) *Polytrichum juniperinum*, in Fire Effect Information System, U.S. Department of Agriculture, Forest Service, Rocky Mountain Research Station, Fire Sciences Laboratory. <http://www.fs.fed.us/database/feis>
- Garonna I, De Jong R, De Wit AJW, Mucher CA, Schmid B, Schaepman ME (2014) Strong contribution of autumn phenology to changes in satellite-derived growing season length estimates across Europe (1982–2011). *Glob Change Biol* 20:3457–3470
- Goulden ML, McMillan AMS, Winston GC, Rocha AV, Manies KL, Harden JW, Bond-Lamberty BP (2010) Patterns of NPP, GPP, respiration, and NEP during boreal forest succession. *Global Change Biol* 17:855–871. <https://doi.org/10.1111/j.1365-2486.2010.02274.x>
- Hansen J, Ruedy R, Sato M, Reynolds R (1996) Global surface air temperature in 1995: return to ore-Pinatubo level. *Geophys Res Lett* 23:1665–1668
- Hicke JA, Asner GP, Kasischke ES, French NHF, Randerson JT, Stocks BJ, Tucker CJ, Los SO, Field CB (2003) Post fire response of North American net primary productivity measured by satellite imagery. In: Johnson D, Kershaw L, MacKinnon A, Pojar J (eds) *Plants of the Western forest. Boreal and Aspen Parkland, Alberta*, pp 1145–1157
- Himzman LD, Fukuda M, Sandberg DV, Chapin FS, Dash D (2003) FORSTFIRE: An experimental approach to predicting the climate feedbacks from the changing boreal fires regime. *H Geophys Res* 108(D1):8154. <https://doi.org/10.1029/2001JD000415>

- Hirose T (2005) Development of the Monsi-Saeki theory on canopy structure and function. *Ann Bot* 95:483–494
- Hogda KA, Tommervik H, Karlsen SR (2013) Trends in the start of the growing season in Fennoscandia 1982–2011. *Remote Sens* 5:4304–4318
- Iio A, Hikosaka K, Anten NPR, Nakagawa Y, Ito A (2014) Global dependence of field-observed leaf area index in woody species on climate: a systematic review. *Glob Ecol Biogeogr* 23:274–285
- IPCC (2014) Climate change 2014: synthesis report. In: Core Writing Team, Pachauri RK and Meyer LA (eds.) Contribution of working groups I, II and III to the fifth assessment report of the intergovernmental panel on climate change, IPCC, Geneva, Switzerland, p 151
- Iwata H, Ueyama M, Harazono Y, Tsuyuzaki S, Kondo M, Uchida M (2011) Quick recovery of carbon dioxide exchanges in a burned black spruce forest in interior Alaska. *SOLA* 7(7):105–108. <https://doi.org/10.2151/sola.2011-027>
- Iwata H, Ueyama M, Harazono Y, Tsuyuzaki S, Kondo M, Uchida M (2011b) Quick recovery of carbon dioxide exchanges in a burned black spruce forest in interior Alaska. *SOLA* 7:105–108
- Iwata H, Ueyama M, Iwama C, Harazono Y (2013) A variation in the fraction of absorbed photosynthetically active radiation and a comparison with MODIS data in burned black spruce forests of interior Alaska. *Polar Sci* 7:113–124
- Jeong S-J, Ho C-H, Gim H-J, Brown ME (2011) Phenology shifts at start vs. end of growing season in temperate vegetation over the Northern Hemisphere for the period 1982–2008. *Glob Change Biol* 17:2385–2399
- Jeong S-J, Medvigy D (2014) Macroscale prediction of autumn leaf coloration throughout the continental United States. *Glob Ecol Biogeogr* 23:1245–1254
- Johnson D, Kershaw L, MacKinnon A, Pojar J (eds) (1995) *Plants of western forest: alaska to Minnesota boreal and aspen parkland*, Lone Pine Publishing, Edmonton
- Kasische ES, Christensen NL, Stocks BR (1995) Fire, global warming, and the carbon balance of boreal forests. *Ecol Appl* 5:437–451
- Kasischke ES (2000) Boreal ecosystems in the global carbon cycle. In: Kasische ES, Stocks BR (eds) *Fire, climate change, and carbon cycling in the Boreal Forest*. Springer, New York, pp 19–30
- Kasische ES, Stocks BR (eds) (2000) *Fire, climate change, and carbon cycling in the boreal forest*, Ecological Studies, vol 138. Springer-Verlag, New York
- Kasischke ES, Stocks BJ, O'Neill K, French NHF, Bourgeau-Chavez LL (2000a) Direct effects of fire on the boreal forest carbon budget. In: Innes JL, Beniston M, Verstraete MM (eds) *Biomass burning and its inter-relationships with the climate system*. Kluwer Academic, Dordrecht, pp 51–68
- Kasischke ES, O'Neill K, Bourgeau-Chavez LL, French NHF (2000b) Indirect and long-term effects of fire on the boreal forest carbon budget. In: Innes JL, Beniston M, Verstraete MM (eds) *Biomass burning and its inter-relationships with the climate system*. Kluwer Academic, Dordrecht, pp 263–280
- Kasischke ES, O'Neill K, French NHF, Bourgeau-Chavez LL (2000c) Controls on patterns of biomass burning in Alaskan boreal forest. In: Innes JL, Beniston M, Verstraete MM (eds) *Biomass burning and its inter-relationships with the climate system*. Kluwer Academic, Dordrecht, pp 173–196
- Kasischke ES, Tanase MA, Bourgeau-Chavez LL, Borr M (2011) Soil moisture limitations on monitoring boreal forest regrowth using spaceborne L-band SAR data. *Remote Sens Environ* 115:227–232
- Keenan TF, Gray J, Friedl MA, Toomey M, Bohrer G, Hollinger DY, Munger W, O'Keefe J, Schmid HP, Wing IA, Yang B, Richardson AD (2014) Net carbon uptake has increased through warming-induced changes in temperate forest phenology. *Nat Clim Change* 4:598–604
- Kim Y, Tanaka N (2003) Effect of forest fire on the fluxes of CO<sub>2</sub>, CH<sub>4</sub>, and N<sub>2</sub>O in boreal forest soils, interior Alaska. *J Geophys Res* 108(D1):8154. <https://doi.org/10.1029/2001JD000663>

- Kim Y, Ueyama M, Nakagawa F, Tsunogai U, Tanaka N, Harazono Y (2007) Assessment of winter fluxes of CO<sub>2</sub> and CH<sub>4</sub> in boreal forest soils of central Alaska estimated by the profile method and the chamber method: a diagnosis of methane emission and implications for the regional carbon budget. *Tellus* 59B:223–233
- Kim Y, Kim SD, Enomoto H, Kushida K, Kondoh M, Uchida M (2013) Latitudinal distribution of soil CO<sub>2</sub> efflux and temperature along the Dalton Highway, Alaska. *Polar Sci* 7:162–173
- Kim Y (2014) Effect of ablation rings and soil temperature on 3-year sprung CO<sub>2</sub> efflux along the Dalton Highway, Alaska. *Biogeosciences* 11:6539–6552. <https://doi.org/10.5194/bg-11-6539-2014>
- Kim Y, Kodama Y, Shim C, Kushida K (2014) Carbon exchange rates in *Polytrichum juniperinum* moss of burned black spruce forest in interior Alaska. *Polar Sci* 8:146–155
- Kobayashi H, Iwabuchi H (2008) A coupled 1-D atmosphere and 3-D canopy radiative transfer model for canopy reflectance, light environment, and photosynthesis simulation in a heterogeneous landscape. *Remote Sens Environ* 112:173–185
- Kobayashi H, Yunus AP, Nagai S, Sugiura K, Kim Y, Van Dam B, Nagano H, Zona D, Harazono Y, Bret-Harte MS, Ichii K, Ikawa H, Iwata H, Oechel W, Ueyama M, Suzuki R (2016) Latitudinal gradient of spruce forest understory and tundra phenology in Alaska as observed from satellite and ground-based data. *Remote Sens Environ* 177:160–170
- Kojima K (2001) Contribution of snow dent around stem on the snowmelt rate in larch forest Japan. *Snow Ice Hokkaido* 20:9–12 (in Japanese)
- Levine JS (1991) Global biomass burning: atmospheric, climate, and biospheric implications. MIT Press, Cambridge
- Le Toan T, Quegan S, Woodward I, Lomas M, Delbart N, Picard G (2004) Relating radar remote sensing of biomass to modelling of forest carbon budgets. *Clim Change* 67:379–402
- Litvak M, Miller S, Wofsy SC, Goulden M (2003) Effect of stand age on whole ecosystem CO<sub>2</sub> exchange in the Canadian boreal forest. *J Geophys Res* 108(3):8225. <https://doi.org/10.1029/2001JD000854>
- Liu H, Randerson JT (2008) Interannual variability of surface energy exchange depends on stand age in a boreal forest fire chronosequence. *J Geophys Res* 113:G01006. <https://doi.org/10.1029/2007JG000483>
- Lloyd J, Taylor JA (1994) On the temperature dependence of soil respiration. *Funct Ecol* 8:315–323
- Lynch JA, Clark JS, Bigelow NH, Edwards ME, Finney BP (2003) Geographic and temporal variations in fire history in boreal ecosystems of Alaska. *J Geophys Res*. <https://doi.org/10.1029/2001JD000332>
- Lyons EA, Jin Y, Randerson JT (2008) Changes in surface albedo after fire in boreal forest ecosystems of interior Alaska assessed using MODIS satellite observations. *J Geophys Res* 113:G02012. <https://doi.org/10.1029/2007JG000606>
- McDonald KC, Kimball JS, Njoke E, Zimmermann R, Zhao M (2004) Variability in springtime thaw in the terrestrial high latitudes: monitoring a major control on the biospheric assimilation of atmospheric CO<sub>2</sub> with spaceborne microwave remote sensing. *Earth Interact* 8:1–23
- Monson RK, Lipson DL, Burns SP, Turnipseed AA, Delany AC, Williams MW, Schmidt SK (2006a) Winter forest soil respiration controlled by climate and microbial community composition. *Nature* 439. <https://doi.org/10.1038/nature04555>
- Monson RK, Burns SP, Williams MW, Delany AC, Weintraub M, Lipson DL (2006b) The contribution of beneath-snow soil respiration to total ecosystem respiration in a high-elevation, subalpine forest. *Global Biogeochem Cycles* 20, GB3030, <https://doi.org/10.1029/2005gb002684>
- Muraoka H, Noda HM, Nagai S, Motohka T, Saitoh TM, Nasahara KN, Saigusa N (2013) Spectral vegetation indices as the indicator of canopy photosynthetic productivity in a deciduous broadleaf forest. *J Plant Ecol* 6:393–407
- Myneni RB, Keeling CD, Tucker CJ, Asrar G, Nemani RR (1997) Increased plant growth in the northern high latitudes from 1981 to 1991. *Nature* 386:698–702

- Myneni RB, Hoffman S, Knyazikhin Y et al (2002) Global products of vegetation leaf area and fraction absorbed PAR from year one of MODIS data. *Remote Sens Environ* 83:214–231
- Nagai S, Saitoh TM, Kurumado K, Tamagawa I, Kobayashi H, Inoue T, Suzuki R, Gamo M, Muraoka H, Nasahara KN (2013) Detection of bio-meteorological year-to-year variation by using digital canopy surface images of a deciduous broad-leaved forest. *Sola* 9:106–110
- Nagai S, Saitoh TM, Nasahara KN, Suzuki R (2015) Spatio-temporal distribution of the timing of start and end of growing season along vertical and horizontal gradients in Japan. *Int J Biometeorol* 59:47–54
- Nagai S, Nasahara KN, Yoshitake S, Saitoh TM (2017) Seasonality of leaf litter and leaf area index data for various tree species in a cool-temperate deciduous broad-leaved forest, Japan, 2005–2014. *Ecol Res* 32:297–297
- Nagai S, Akitsu T, Saitoh TM et al (2018) 8 million phenological and sky images from 29 ecosystems from the Arctic to the tropics: the phenological eyes network. *Ecol Res* 33:1091–1092
- Nagumo H, Minowa M (1990) *Sokujugaku (Dendrometry)*. Chikyusha, Tokyo, Japan, p 243
- Nasahara KN, Muraoka H, Nagai S, Mikami H (2008) Vertical integration of leaf area index in a Japanese deciduous broad-leaved forest. *Agric For Meteorol* 148:1136–1146
- Oechel WC, Vourlitis GL (1997) Climate change in northern latitudes: alterations in ecosystem structure and function and effects on carbon sequestration. In: Oechel WC, Callaghan T, Gilmanov T, Holten JL, Maxwell B, Molau U, Svebjörnsson B (eds) *Global change and Arctic terrestrial ecosystems*. Springer, New York, pp 381–401
- Oechel WC, Laskowski CA, Burba G, Gioli B, Kalhori AAM (2014) Annual patterns and budget of CO<sub>2</sub> flux in an Arctic tussock tundra ecosystem. *J Geophys Res Biogeosci* 119:323–339
- O'Neill KP, Kasischke ES, Richter DD (2003) Seasonal and decadal patterns of soil carbon uptake and emission along an age-sequence of burned black spruce forest stands in interior Alaska. *J Geophys Res* 108(D1):8155. <https://doi.org/10.1029/2001JD000443>
- O'Neill KP, Richter DD, Kasischke ES (2006) Succession-driven changes in soil respiration following fire in black spruce stands of interior Alaska. *Biogeochemistry* 80:1–20
- Osumi S (1987) *Shinrin keisoku-gaku kogi (Lecture on forest dendrometry)*. Yokendo, Tokyo, Japan, p 287
- Piao S, Wang X, Ciais P, Zhu B, Wang T, Liu J (2011) Changes in satellite-derived vegetation growth trend in temperate and boreal Eurasia from 1982 to 2006. *Glob Change Biol* 17:3228–3239
- Pisek J, Chen JM (2009) Mapping forest background reflectivity over North America with Multi-angle Imaging SpectroRadiometer (MISR) data. *Remote Sens Environ* 113:2412–2423
- Potitthep S, Nagai S, Nasahara KN, Muraoka H, Suzuki R (2013) Two separate periods of the LAI–VIs relationships using in situ measurements in a deciduous broadleaf forest. *Agric For Meteorol* 169:148–155
- Randerson JT et al (2006) The impact of boreal forest fire on climate warming. *Science* 314:1130–1132
- Rautiainen M, Heiskanen J (2013) Seasonal contribution of understory vegetation to the reflectance of a boreal landscape at different spatial Scales. *IEEE Geosci Remote Sens Lett* 10:923–927
- Raynolds MK, Walker DA, Maier HA (2006) Alaska arctic tundra vegetation map. Scale 1:4,000,000. Conservation of Arctic Flora and Fauna (CAFF) Map No. 2. U.S. Fish and Wildlife Service, Anchorage, Alaska
- Rayment MB, Jarvis PG (2000) Temporal and spatial variation of soil CO<sub>2</sub> efflux in a Canadian boreal forest. *Soil Biol Biochem* 32:35–45
- Richardson AD, Dail DB, Hollinger DY (2011) Leaf area index uncertainty estimates for model–data fusion applications. *Agric For Meteorol* 151:1287–1292
- Richardson AD, Jenkins JP, Braswell BH, Hollinger DY, Ollinger SV, Smith ML (2007) Use of digital webcam images to track spring green-up in a deciduous broadleaf forest. *Oecologia* 152:323–334

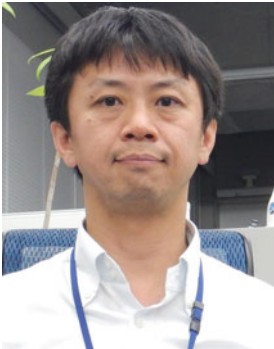
- Richardson AD, Keenan TF, Migliavacca M, Ryu Y, Sonnentag O, Toomey M (2013a) Climate change, phenology, and phenological control of vegetation feed-backs to the climate system. *Agric For Meteorol* 169:156–173
- Richardson AD, Carbone MS, Keenan TF, Czimczik CI, Hollinger DY, Murakami P, Schaberg PG, Xu X (2013b) Seasonal dynamics and age of stemwood nonstructural carbohydrates in temperate forest trees. *New Phytol* 197:850–861
- Richter DD, O'Neill KP, Kasischke ES (2000) Postfire stimulation of microbial decomposition in black spruce (*Picea mariana* L.) forest soils: a hypothesis. In: Kasischke ES, Stocks BR (eds) *Fire, climate change, and carbon cycling in the Boreal Forest*. Springer, New York, pp 173–196
- Risk D, Nickerson N, Creelman C, McArthur G, Owens J (2011) Forced diffusion soil flux: A new technique for continuous monitoring of soil gas efflux. *Agr For Meteorol* 151:1622–1631
- Rosenqvist A, Shimada M, Ito N, Watanabe M (2007) ALOS PALSAR: a pathfinder mission for global-scale monitoring of the environment. *IEEE Trans Geosci Remote Sens* 45:3307–3316
- Ruokolainen L, Salo K (2006) The succession of boreal forest vegetation during ten years after slash-burning in Koli National Park, eastern Finland. *Ann Bot Fennici* 43:363–378
- Ryu Y, Sonnentag O, Nilson T, Vargas R, Kobayashi H, Wenk R, Baldocchi DD (2010) How to quantify tree leaf area index in an open savanna ecosystem: a multi-instrument and multi-model approach. *Agric For Meteorol* 150:63–76
- Savage KE, Davidson EA (2003) A comparison of manual and automated systems for soil CO<sub>2</sub> flux measurements: trade-offs between spatial and temporal resolution. *J Exper Botany* 54:891–899
- Schlentner RE, Van Cleve K (1985) Relationships between CO<sub>2</sub> evolution from soil, substrate temperature, and substrate moisture in four mature forest types in interior Alaska. *Can J For Res* 15:97–106
- Schlesinger WH (1997) *Biogeochemistry: an analysis of global change*. Academic, San Diego, California
- Schlesinger WH, Andrews JA (2000) Soil respiration and the global carbon cycle. *Biogeochemistry* 48:7–20
- Schmidt SK, Costello EK, Nemergut DR, Cleveland CC, Reed SC, Weitraub MN, Meyer AF, Martin AM (2007) Biogeochemical consequences of rapid microbial turnover and seasonal succession in soil. *Ecology* 88:1379–1385
- Schimmel J, Granstrom A (1996) Fire severity and vegetation response in the boreal Swedish forest. *Ecology* 77:1436–1450
- Schwartz MD, Ault TR, Betancourt JL (2013) Spring onset variations and trends in the continental United States: past and regional assessment using temperature-based indices. *Int J Climatol* 33:2917–2922
- Seiler W, Crutzen PJ (1980) Estimates of gross and net fluxes of carbon between the biosphere and atmosphere from biomass burning. *Clim Change* 2:207–247
- Shimada M (2010) Ortho-rectification and slope correction of SAR data using DEM and its accuracy evaluation. *IEEE J Sel Topics Appl Earth Observ Remote Sens* 3:657–671
- Shimada M, Isoguchi O, Tadono T, Isono K (2009) PALSAR radiometric and geometric calibration. *IEEE Trans Geosci Remote Sens* 47:3915–3932
- Skutch AF (1929) Early stages of plant succession following forest fires. *Ecology* 10:177–190
- Sommerfeld RA, Mosier AR, Musselman RC (1993) CO<sub>2</sub>, CH<sub>4</sub> and N<sub>2</sub>O flux through a Wyoming snowpack and implications for global budgets. *Nature* 361:140–142
- Stocks BJ, Mason JA, Todd JB, Bosch EM, Wotton BM, Amiro BD, Flannigan MD, Hirsch KG, Logan KA, Martell DL, Skinner WR (2003) Large forest fires in Canada, 1959–1997. *J Geophys Res.* <https://doi.org/10.1029/2001JD000484>
- Sturm M, Schimmel J, Michaelson G, Welker JM, Oberbauer SF, Liston GE, Fahnestock J, Romanovsky V (2005) Winter biological processes could help convert Arctic tundra to shrubland. *Biosci* 55:17–26

- Sugiura K, Nagai S, Nakai T, Suzuki R (2013) Application of time-lapse digital imagery for ground-truth verification of satellite indices in the boreal forests of Alaska. *Polar Sci* 7:149–161
- Suzuki R, Kim Y, Ishii R (2013) Sensitivity of the backscatter intensity of ALOS/PALSAR to the above-ground biomass and other biophysical parameters of boreal forest in Alaska. *Polar Sci* 7 (2):100–112
- Tsuyuzaki S, Kushida K, Kodama Y (2009) Recovery of surface albedo and plant cover after wildfire in a *Picea mariana* forest in interior Alaska. *Clima Change* 93:517–525
- Tsuyuzaki S, Narita K, Sawada Y, Harada K (2013) Recovery of forest-floor vegetation after a wildfire in a *Picea mariana* forest. *Ecol Res* 28:1061–1068
- Ueyama M, Harazono Y, Ohtaki E, Miyata A (2006) Controlling factors on the interannual CO<sub>2</sub> budget at a subarctic black spruce forest in interior Alaska. *Tellus B Chem Phys Meteorol* 58 (5):491–501
- Ueyama M et al (2013) Upscaling terrestrial carbon dioxide fluxes in Alaska with satellite remote sensing and support vector regression. *J Geophys Res Biogeosci* 118:1–16. <https://doi.org/10.1002/jgrg.20095>
- Ueyama M et al (2014) Change in surface energy balance in Alaska due to fire and spring warming, based on upscaling eddy covariance measurements. *J Geophys Res Biogeosci* 119:1947–1969. <https://doi.org/10.1002/2014JG002717>
- Ulaby FT, Moore RK, Fung AK (1986) *Microwave remote sensing: active and passive*, volume III: from the theory to applications. Artech House, Norwood, MA, USA, p 2162
- Van Cleve K, Dryness CT, Viereck LA, Fox J, Chapin FS, Oechel W (1983) Taiga ecosystems in interior Alaska. *Bioscience* 33:39–44
- Verbyla D (2008) The greening and browning of Alaska based on 1982–2003 satellite data. *Glob Ecol Biogeogr* 17:547–555
- Viereck LA, Dyrness CT, Batten AR, Wenzlick KJ (1992) *The Alaska vegetation classification*. Gen. Tech. Rep. PNW-GTR-286. Portland, OR: U.S. Department of Agriculture, Forest Service, Pacific Northwest Research Station
- Vitt DH, Marsh JE, Bovey RB (eds) (1988) *Mosses, Lichens and Ferns of Northwest North America*. Alberta, Canada
- White MA, Thornton PE, Running SW (1997) A continental phenology model for monitoring vegetation responses to interannual climatic variability. *Global Biogeochem Cycles* 11:217–234
- Winston GC, Sundquist ET, Stephens BB, Trumbore SE (1997) Winter CO<sub>2</sub> fluxes in a boreal forest. *J Geophys Res* 102:28795–2880
- Woebbecke DM, Meyer GE, Vonbargen K, Mortensen DA (1995) Color indexes for weed identification under various soil, residue, and lighting conditions. *Trans Asae* 38:259–269
- Xu L, Myneni RB, Chapin FS III, Callaghan TV, Pinzon JE, Tucker CJ, Zhu J, Bi J, Ciais P, Tommervik H, Euskirchen ES, Forbes BC, Piao SL, Anderson BT, Ganguly S, Nemani RR, Goetz SJ, Beck PSA, Bunn AG, Cao C, Stroeve JC (2013) Temperature and vegetation seasonality diminishment over northern lands. *Nat Clim Change* 3:581–586
- Xu M, Qi Y (2001) Soil-surface CO<sub>2</sub> efflux and its spatial and temporal variations in a young ponderosa pine plantation in northern California. *Global Change Biol* 7:667–677
- Yarie J (1981) Forest fire cycles and life tables: a case study from interior Alaska. *Can J For Res* 11:554–562
- Yarie Y, Kane E, Mack M (2007) Aboveground biomass equations for the trees of interior Alaska. *Agricult For Exper Station Bull* 115:1–16
- Yang W, Kobayashi H, Suzuki R, Nasahara KN (2014) A simple method for retrieving understory NDVI in sparse needleleaf forests in Alaska using MODIS BRDF data. *Remote Sens* 6:11936–11955
- Yang W, Kobayashi H (2018) Satellite estimation of overstory and understory LAI in boreal forests: a research land product of JAXA GCOM-C project. In: *Proceedings of the 64th spring conference of the remote sensing society of Japan*, Kashiwa Campus of the University of Tokyo, pp 95–96

- Zhang XY, Friedl MA, Schaaf CB, Strahler AH, Hodges JCF, Gao F, Reed B, Huete A (2003) Monitoring vegetation phenology using MODIS. *Remote Sens Environ* 84:471–475
- Zhu WQ, Tian HQ, Xu XF, Pan YZ, Chen GS, Lin WP (2012) Extension of the growing season due to delayed autumn over mid and high latitudes in North America during 1982–2006. *Glob Ecol Biogeogr* 21:260–271
- Zhu Z, Bi J, Pan Y, Ganguly S, Anav A, Xu L, Samanta A, Piao S, Nemani RR, Myneni RB (2013) Global data sets of vegetation leaf area index (LAI)3 g and fraction of photosynthetically active radiation (FPAR)3g derived from global inventory modeling and mapping studies (GIMMS) normalized difference vegetation index (NDVI3g) for the period 1981 to 2011. *Remote Sens* 5:927–948



**Dr. Yongwon Kim** received the Ph.D. degree in the Graduate School of Environmental Earth Science from the Hokkaido University, Sapporo, Japan in 1998. He was a Postdoctoral Fellow in the Japan Aerospace Exploration Agency (JAXA), the Japan Agency for Marine-Earth Science and Technology (JAMSTEC), Japan, and the International Arctic Research Center (IARC) of the University of Alaska Fairbanks (UAF), USA. He is currently a Research Associate Professor in the IARC of UAF. His main research concerns are to quantify soil carbon emission in response to changes in climate and environment in the Sub-Arctic and Arctic terrestrial ecosystems.



**Dr. Hideki Kobayashi** received the Ph.D. degree in Environmental Science and Technology from Tokyo Institute of Technology, Tokyo, Japan in 2004. He was a Postdoctoral Fellow in Japan Agency for Marine-Earth Science and Technology (JAMSTEC) and University of California, Berkeley. He is currently a Deputy Research Unit Leader in Institute of Arctic Climate and Environmental Research, JAMSTEC, and also serves as Adjunct Associate Professor at Tokyo Institute of Technology and Visiting Associate Professor at Chiba University. His recent research interests are in plant canopy radiative transfer and integration of the near-surface, airborne and satellite remote sensing of plant canopies with particular focus on northern high latitudes.



**Dr. Shin Nagai** defended the Ph.D. degree in the Graduate School of Environmental Studies from the Nagoya University, Nagoya, Japan in 2007. He was a Postdoctoral Fellow in the Gifu University, Gifu, Japan. Currently, he is a Senior Scientist in the Research Institute for Global Change of Japan Agency for Marine-Earth Science and Technology (JAMSTEC), Yokohama, Japan. His main research concerns are to evaluate the spatio-temporal variability of plant phenology in response to changes in climate and environment in the Arctic, temperate, and tropical ecosystems by remote sensing observations.



**Dr. Masahito Ueyama** is an Associate Professor of Graduate School of Life and Environmental Sciences of Osaka Prefecture University in Sakai, Japan. His research interest is the land-atmosphere interaction of energy, water, and trace gases. His approach relies on integration and synthesis of field observations, numerical model, and remote sensing data. Dr. Ueyama received his Doctoral degree in Science at Graduate School of Natural and Technology, Okayama University, and worked at International Arctic Research Center, University of Alaska, Fairbanks, USA as a visiting research scholar.



**Dr. Bang Yong Lee** Lee received the Ph.D. degree in the Graduate School of Atmospheric Sciences from the Yonsei University, Seoul, Korea in 2000. He is currently a Senior Research Scientist in the Korea Polar Research Institute (KOPRI). His main research concerns are to understand the process of greenhouse gas exchange between climate, ecosystem, and frozen soil, and combined with satellite exploration to improve the accuracy of environmental change forecast across the entire scale of the Pan-Arctic permafrost regions.



**Dr. Rikie Suzuki (the deceased)** received the Ph.D. degree in the Climate and Meteorology from the University of Tsukuba in 1989. From 1989 to 1998, he was a Postdoctoral Fellow, Research Associate, and Assistant Professor in University of Tsukuba. In 1998, he joined the Frontier Research System for Global Change. In 2004, he joined the Japan Agency for Marine-Earth Science and Technology (JAMSTEC) and served as a Senior Researcher, Team Leader, and Director until 2017. He also served as an associated editor in Polar Science Journal, Chigaku Zasshi (In Japanese) and a committee member in Earth and Planetary Science Division of Science Council of Japan. His past research interests were in geographical analysis of climate and plant interactions using remote sensing and climate data sets. His research target was on the Eastern Siberia and Alaska. He experienced and led several field-work projects in China, Mongolia, Siberia, and Alaska.



# Northern Ecohydrology of Interior Alaska Subarctic

# 22

Jessica M. Young-Robertson, W. Robert Bolton, and Ryan Toohey

## Abstract

Ecohydrology—as an interdisciplinary field—developed in and explores processes in warm semi-arid and arid ecosystems. This field is in its infancy with respect to arctic and subarctic systems in Alaska. However, similar to warm and dry regions, soil moisture storage is a driver of ecohydrological processes in these northern regions. The presence or absence of permafrost impacts soil moisture storage and determines whether ecological or hydrological processes drive water cycling. The arctic is in the zone of continuous permafrost distribution, and the subarctic is in the zone of discontinuous permafrost distribution. In the subarctic, hydrological processes are dominated by soil moisture storage in areas with permafrost and by ecological processes in areas without permafrost. Given the infancy of the ecohydrology discipline in arctic and subarctic systems, there are a number of knowledge gaps outlined at the end of this chapter.

## Keywords

Boreal forest · Alaska · Birch · Black spruce · Soil storage · Active layer · Permafrost

J. M. Young-Robertson (✉)

Agricultural and Forestry Experiment Station, Institute of Agriculture, Natural Resources and Extension, University of Alaska Fairbanks, Fairbanks, AK, USA  
e-mail: [jmrobertson3@alaska.edu](mailto:jmrobertson3@alaska.edu)

W. R. Bolton

International Arctic Research Center, University of Alaska Fairbanks, Fairbanks, AK, USA  
e-mail: [wrbolton@alaska.edu](mailto:wrbolton@alaska.edu)

R. Toohey

Alaska Climate Adaptation Science Center, Anchorage, AK, USA  
e-mail: [rtoohey@usgs.gov](mailto:rtoohey@usgs.gov)

© Springer Nature Switzerland AG 2021

D. Yang and D. L. Kane (eds.), *Arctic Hydrology, Permafrost and Ecosystems*,  
[https://doi.org/10.1007/978-3-030-50930-9\\_22](https://doi.org/10.1007/978-3-030-50930-9_22)

657

## 22.1 Introduction

Ecohydrology is an interdisciplinary field that examines the soil–plant–atmosphere continuum, and specifically focuses on the hydrological processes that drive ecological processes. The field of ecohydrology has largely developed based on the water balance processes in desert regions, which experience high evaporation rates and potential evapotranspiration (PET), high competition for water among plants, strong wet–dry soil moisture dynamics, and high water stress. According to an ecohydrology review by Rodriguez-Iturbe (2000), soil moisture is the link for the plant–atmosphere continuum and for integrating the spatiotemporal dynamics of ecological and hydrological processes. Soil moisture storage can act as a reservoir for plants to utilize and support them during periods of low rainfall. This is true for desert and non-desert regions, such as Alaskan arctic and subarctic systems that will be discussed herein.

Permafrost is defined as ground (soil, rock, sediment) that is frozen ( $<0$  °C) for two or more consecutive years. Near-surface permafrost resides below a thin (typically  $<1$  m thick) seasonally frozen and thawed soil layer (the “active layer”) (Pastick et al. 2015). In the zone of discontinuous permafrost (mostly subarctic), permafrost is found primarily on north facing slopes and valley bottoms (Jorgenson et al. 2010). Within Alaskan arctic and subarctic systems, which are located in the zone of continuous and discontinuous permafrost, storage dynamics—such as seasonal soil freeze–thaw, the presence or absence of permafrost, snow accumulation and ablation, and tree water dynamics—dominate hydrological processes. However, these mechanisms and processes of storage dynamics are an active and expanding research area. Some of the knowledge gaps in these areas limit accurate modeling and predicting of changes in hydrology (Bring et al. 2016). Storage is defined as water detained within a watershed. Storage mechanisms include soil moisture, groundwater, lake and ponds, and snow/glaciers, etc. It is critical to determine the storage capacity of soils and vegetation in Arctic and subarctic systems. In some hydrological models, storage can be included in a vaguely defined error term, which can include uncertainties associated with other aspects of the water balance (precipitation, evapotranspiration, plant storage, and discharge). It can be challenging to predict changes in water balance if vague error terms (that lack mechanistic functions) describe storage in a storage-dominated system. Further, error propagation into model estimates can be large when scaling water balance to the landscape level because the storage terms are not well quantified or mechanistically understood. Permafrost, hydrology, ecosystem water use, and climate are tightly interconnected and impact storage processes. However, understanding their interconnectedness has rarely been approached in a holistic manner in field or modeling research. The largely disciplinary approach taken thus far further hinders modeling efforts aimed at capturing the impact of climate change and permafrost thaw on ecosystems. Changes in storage—due to thawing permafrost, change in vegetation communities, snow accumulation and ablation, and deepening of the active layer—has implications for stream flow and ultimately freshwater

export from the boreal forest (McGuire et al. 2006; McGuire and Chapin 2006). Implications of storage change also exist for tree resistance to drought, snowmelt water pathways, groundwater recharge in permafrost-free areas, fish population, atmospheric moisture, and climate. The presence or absence of ice-rich permafrost is *the* primary control on the processes impacting hydrology and ecology in subarctic systems (Kane et al. 2008; Hinzman et al. 2005, 2006a, b; Jorgenson et al. 2013). See Fig. 22.1.

---

## 22.2 Permafrost and Ecohydrology

The presence or absence of permafrost impacts the ecosystem and its components. Areas underlain with ice-rich permafrost have relatively cold, wet soils and thick organic layers that support an extensive non-vascular plant community (mosses) and, in the subarctic, small-statured black spruce trees (*Picea mariana*). Permafrost-free areas (in the subarctic), with relatively dry, warm soils and thin organic layers, support large deciduous trees (primarily *Betula neoalaskana* and *Populus tremuloides*), along with some understory shrubs, herbaceous plants, and white spruce (*Picea glauca*). Each of these ecosystems has different water use strategies and, thus, different water pathways (i.e., vertical vs. horizontal). Hydrological, rather than ecological, processes appear to dominate the ecohydrology of areas with ice-rich permafrost, wherein the understory species and black spruce have low water use rates and water storage, with transpiration rates around 10–50 mL water day<sup>-1</sup> (black spruce, Young-Robertson pers obs) and stem water contents around 25–50% (Young-Robertson et al. 2016, Fig. 22.2). The dominant water pathway is lateral, or horizontal, through the soil as ice-rich permafrost effectively creates an aquitard due to its reduced permeability (Dingman 1975; Woo and Marsh 1990; Woo 2012). This prevents near-surface waters from percolating into deeper soils, thereby forcing near-surface water to move laterally over the ice-rich soils and into the streams in the valley bottoms.

Conversely, ecological rather than hydrological, processes dominate the ecohydrology of permafrost-free areas. Deciduous trees have very high water use rates and water storage, with transpiration rates nearly an order of magnitude greater than the black spruce and water contents around 75–100% (Young-Robertson et al. 2016, Fig. 22.2). The dominant water pathway is vertical, wherein water either moves into the trees or down through the soil as it percolates into groundwater (Fig. 22.3). Evapotranspiration is discussed with respect to partitioning in the next section and with more discussion on storage in Sect. 22.2.

### 22.2.1 Evapotranspiration Process and Its Impact

In northern environments, growing season and snow cover duration often provide the initiation and termination bounds of the evapotranspiration (ET) flux with soil

	<b>permafrost</b>	
	absent	present
	<b>ecology dominates ecohydrology</b>	<b>hydrology dominates ecohydrology</b>
<b>Alaskan landscape</b>	36 ?? %	18.3 ?? %
<b>primary tree type</b>	deciduous	coniferous
<b>plant water use</b>	high	low
<b>evapotranspiration partitioning</b>	transpiration	evaporation
<b>water storage compartment</b>	trees and deep groundwater	soil / active layer
<b>primary water pathway</b>	vertical	horizontal
<b>primary hydrological processes</b>	transpiration and groundwater recharge	streamflow and evaporation
<b>primary climate change threats</b>	reduced snowpack	disturbance and permafrost thaw
<b>drought buffering mechanism</b>	tree water storage	soil water storage, antecedent moisture
<b>drought tolerance</b>	high	low
<b>climate equivalent</b>	semi-arid	mesic



←
 In the boreal forest, disturbance that thaws permafrost favors deciduous plant establishment and, thus, ecologically dominated ecohydrology